Journal of Inflammation Research

Dovepress
open access to scientific and medical research

Open Access Full Text Article

ORIGINAL RESEARCH

Melatonin Suppresses NLRP3 Inflammasome Activation via TLR4/NF-κB and P2X7R Signaling in High-Fat Diet-Induced Murine NASH Model

Moumita Saha[1], Krishnendu Manna[2], Krishna Das Saha[1]

[1]Cancer Biology and Inflammatory Disorder Division, CSIR-Indian Institute of Chemical Biology, Kolkata, West Bengal, India; [2]Department of Food and Nutrition, University of Kalyani, Kalyani, West Bengal, India

Correspondence: Krishna Das Saha, Cancer Biology and Inflammatory Disorder Division, CSIR-Indian Institute of Chemical Biology, 4 Raja S.C. Mullick Road, Kolkata, West Bengal, 700032, India, Tel +91 33 2499 5810, Fax +91 33 2473 5197, Email krishna@iicb.res.in

Background: NLRP3 inflammasome activation plays a critical role in mediating inflammation and NASH (non-alcoholic steatohepatitis) progression that ultimately leads to cirrhosis and hepatocellular carcinoma. Melatonin (MLT) controls high-fat diet-induced NASH in the murine model by modulating NLRP3 mediated inflammation. P2X7R-mediated inflammasome activation is reported in several inflammatory models including NASH.

Objective: The role of MLT in P2X7R-mediated inflammation in the NASH model has not yet been explored. The present study investigated the role of MLT in amending high-fat diet-induced nonalcoholic steatohepatitis in the murine liver.

Methods: To evaluate the hepatological changes, mice were divided into four groups to investigate the improvement potential of this MLT (10 and 20 mg/kg) and to assess the experimental findings. Histology, biochemical assays, ELISA, FACS analysis, Western blotting, and IF were performed to assess the physical and molecular changes upon melatonin treatment.

Results: The result demonstrated that MLT administration reduced HFD (high-fat diet)-induced non-alcoholic steatohepatitic indices, which successively restored the hepatic morphological architecture and other pathophysiological features too. Moreover, the application of MLT suppressed HFD-induced activation of the inflammasome and through TLR4/NF-κB signaling. Herein, we report that MLT significantly suppresses P2X7R expression and calcium influx along with inflammasome in both in vitro and in vivo. The docking study revealed a strong binding affinity of MLT with P2X7R. Moreover, the results also showed that the Nrf2 level was boosted which may normalize the expression of antioxidant proteins that safeguard against oxidative damage triggered by inflammation. Furthermore, some matrix metalloproteinases like MMP 2 and MMP 9 were repressed and TIMP-1 level was increased, which also signifies that MLT could improve liver fibrosis in this model.

Conclusion: Based on our findings, this study may conclude that MLT could be used as a therapeutic agent in the high-fat diet-induced NASH model as it has persuasive anti-inflammatory potential.

Keywords: melatonin, NASH, NAFLD, inflammasome, P2X7, inflammation, Kupffer cells

Introduction

Metabolic syndrome indicates a group of interrelated metabolic factors, such as dyslipidemia, central obesity, an elevation of arterial serum pressure, insulin resistance, and dysregulated glucose homeostasis, which further confers a higher risk for cardiac diseases (cardiovascular disease; CVD), kidney diseases (chronic kidney disease; CKD) and NAFLD (non-alcoholic fatty liver disease).[1,2] NAFLD covers a broad range of spectrum of hepatic injuries, including steatosis, non-alcoholic steatohepatitis (NASH), cirrhosis, fibrosis, liver failure, and even results in hepatocellular carcinoma.[3] A recent study reveals that the number of NAFLD patients is increasing globally (~25% of the total population) due to unhealthy food habits associated with a sedentary lifestyle.[4] Among all these, NASH is most prevalent in western countries.[5] Various clinical investigations suggest that hepatic injury is a result of massive fat accumulation in the hepatocytes, and that it plays a critical role in the development of NAFLD.[6–8] Nutritional overload to the liver

Received: 15 October 2021
Accepted: 29 March 2022
Published: 31 May 2022

Graphical Abstract

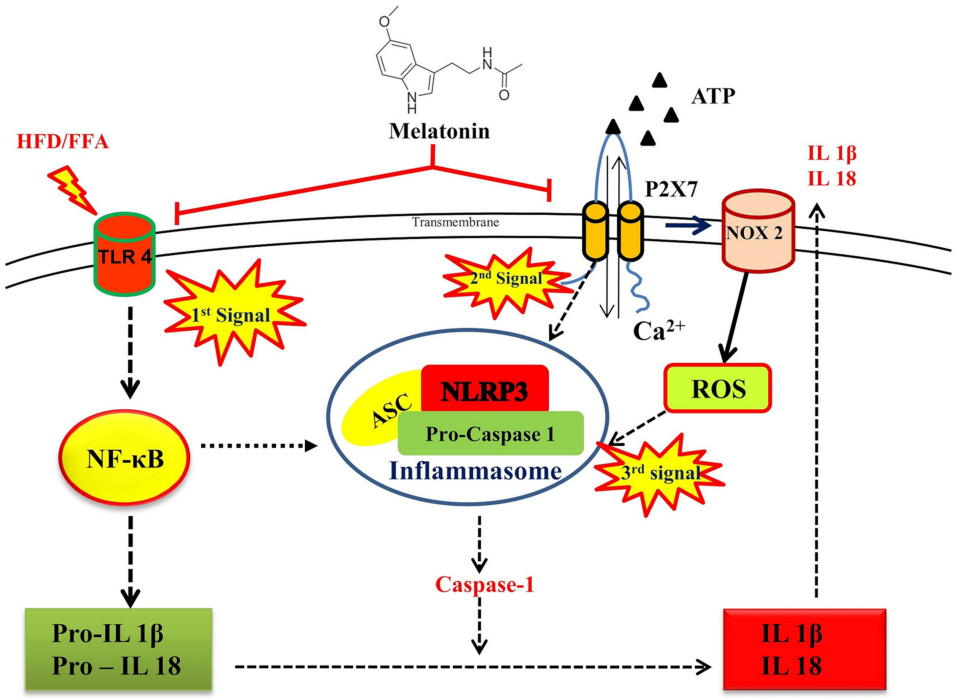

promotes chronic metabolic inflammation, increased rate of oxidative stress, endoplasmic reticulum (ER) stress, and mitochondrial discrepancy.[8–10] The "multiple hit" hypothesis has been proposed in the conversion of NAFLD to NASH.[11] The hits are simple steatosis that causes insulin resistance, steatosis development, rise in adipose tissue-derived hormones, gut microbiota development, upregulation of genetic and epigenetic factors, and other multifaceted processes including oxidative stress, ER stress, inflammation, mitochondrial dysfunction, and lipid peroxidation.[9,12] All these factors cumulatively give rise to NAFLD from NASH.

The pathophysiology and clinical implications of the molecular discrepancies in NASH are both intricate and multifarious. Excessive fat accumulation in the liver occurs mainly due to increased DNL (de-novo lipogenesis) from excess carbohydrates, increased delivery of nutritional fat to the liver from the gut, unbalanced gut physiology, and augmented influx of free fatty acids from the system (primarily from visceral adipose tissue).[13]

The NLRP3 (NLR family pyrin domain containing 3) inflammasome is an abundant intracellular multi-protein scaffold consisting of NOD-like receptor molecules; adaptor proteins like ASC (apoptosis-associated speck-like protein containing a CARD, which is apoptosis-coupled spec-like protein that contains a caspase recruitment domain) and the precursor pro-caspase-1. Activation of this complex causes programmed cell death (pyroptosis), inflammation, and fibrosis.[14] Gut microbiota, different PAMP (pathogen-associated molecular pattern) molecules (LPS; lipopolysaccharide), and lipotoxicity also trigger the inflammasome activation.[15] The activation involves different pathways, such as toll-like receptor (TLR) mediated upregulation of pro-cytokines, ATP-dependent P2X7 receptor activation, and increase in endogenous reactive oxygen species (ROS). Activation of the inflammasome scaffold leads to the maturation of Pro-IL-1β and Pro-IL-18 and these mature cytokines get released from the cell.[14,16–18] Recently, it has been reported that the expression of NLRP3 and its components get significantly increased both in murine and humans with NASH.[19–22]

Melatonin (*N*-acetyl-5-methoxytryptamine, MLT) is generally synthesized from tryptophan by the pineal gland in mammals and humans, at night, and also by the intestinal enterochromaffin cells, which reach the liver through the portal vein. MLT is critical for the synchronization of circadian and seasonal rhythms, pubertal development, and a vital

regulator of energy metabolism in many animals.[23] MLT is also involved in supervising mood control, reproduction, immune system, free radical scavenging, and tumor biology.[24] Furthermore, MLT acts as a highly effective antioxidant and anti-inflammatory molecule.[25,26] Recent evidence suggests that MLT significantly regulates lipid metabolism in the liver.[27,28] Several previous investigations indicated that MLT might contribute to the pathophysiology of NAFLD and attenuation of NASH. However, the precise molecular mechanism underlying this remains indistinct.

In this study, we show that MLT restores the liver cytoarchitecture and exerts potent anti-inflammatory actions in in vivo and in vitro models of NASH. Then, we suggested that Melatonin may act as a valuable defensive alternative strategy for minimizing NASH by inhibiting the activation of the NLRP3 (NACHT, LRR, and PYD domain-containing protein 3) inflammasome signaling, through the interference of P2X7.

Materials and Methods

Chemicals

Melatonin (Cat. no-70902, Cas no. 73-31-4) and Palmitic acid (cat no. 34262) were obtained from Sisco research laboratories (SRL, India). Oleic acid (cat no. O1008) was purchased from Sigma-Aldrich. NF-κB (sc-8008), pNF- κB (sc-136548), TLR 4 (sc-30002), P2X7 (sc-514962), IL-6 (sc-28343), IL-18 (sc-7954), Il-1β (sc-7884), β-Actin (sc-47778), TNF-α (sc-1350), ASC (sc-514414), Timp-1 (sc-21734), NOX-2 (SC-130543) and Caspase-1 (sc-56036) antibodies were procured from Santa Cruz Biotechnology. MMP2 (#87809), MMP-9 (#13667), and α – tubulin (#2144) antibodies were purchased from Cell Signaling Technology. NLRP3 (ab4207) was procured from Abcam. Primary tagged antibodies of FITC-F4/80, Pro-Il-1β, and CD11b were procured from Invitrogen. High Fat Diet (cat no. 296024210) was procured by MP Biomedicals.

Cell Culture and Induction of Steatosis in HepG2 Cells with Oleic and Palmitic Acids

The human hepatocellular carcinoma cell line (HepG2) was purchased from NCCS, Pune, and was cultured in complete DMEM [10% (v/v) FBS and 1% PSN]. The cells were maintained in a humidified condition in an incubator maintaining 5% $CO_2$and 37°C. Oleic acid (OA) and palmitic acid (PA) were used to establish the cellular fatty liver/hepatic steatosis model.[29] The PA was dissolved in ethanol, and then OA/PA was mixed at 2:1 ratio (2 mM). The mixture was then dissolved in BSA and vibrated overnight at 37°C. The solution mixture was prepared freshly before each experiment. MLT is dissolved in DMEM culture medium and was treated with cells at different concentrations for further experiments. According to previous reports,[30–32] 50 μmol/L Glyburide and 10 nM Brilliant Blue G (BBG), were used in the study, as their final concentrations.

MTT Assay

This in vitro assay estimates the reduction of MTT by mitochondrial succinate dehydrogenase enzyme. MTT enters the mitochondria and gets reduced to an insoluble, colored (dark purple) formazan product. The formazan was solubilized with DMSO (an organic solvent), and the released solubilized reagent was measured by a spectrophotometer. This assay has been performed to determine the cytotoxic effect of MLT. Cells were seeded in a 96-well plate and treated with different concentrations of MLT (50,100, 200, 400, 800, and 1600 μM dissolved in a complete DMEM) and the plate was kept in the incubator for 24 h. After incubation, MTT (4 mg/mL) reagent was added, and the plate was further incubated for an additional 4 h. The absorbance of DMSO-solubilized formazan has been taken at a wavelength of 595 nm using an ELISA reader.

Animals and Experimental Protocol

Wild-type male C57BL/6 (20–22 g) mice were procured from the CSIR-India Institute of Chemical Biology animal house. The mice were kept in standard laboratory conditions with access to food and water, under a sterile environment for one week, before starting experimental procedures, and they were allowed to adapt to the new environment. All of the experiments were carried out following the Institutional Animal Care and Use Committee guidelines and permitted by

the Institutional Ethics Committee (IEC) of CSIR-Indian Institute of Chemical Biology. All the experiments were carried away in the dissection room of the institutional animal house.

Non-Alcoholic Steatohepatitis (NASH) Model

After acclimatization for one week, 20 mice were divided into 5 subgroups and they were treated with MLT at different doses (NCD, 10, 20, 40, 80 mg/kg body weight) for 1 month. Following a preliminary experiment, 10 mg/kg and 20 mg/kg doses were selected for the further experimental procedure. Thirty experimental mice were arbitrarily divided into several subgroups, such as control, High Fat Diet (HFD), HFD + MLT D1 (10 mg/kg), HFD+ MLT D2 (20 mg/kg). A high-fat diet was given to the mice groups and MLT (dissolved in 1XPBS) was administered by i.p. (intraperitoneal) injection every alternate day, for 6 months and an equal volume of 1XPBS was injected to the control group of mice. Mice had unrestricted access to food and water, and bodyweight was recorded monthly. At the end of the experiment, all the animals were anesthetized by an intraperitoneal injection of 100 mg/kg Ketamine and 10 mg/kg xylazine hydrochloride and sacrificed via cervical dislocation to collect the serum and plasma, which were stored at −20 °C for further experimental analysis. Livers were dissected out, weighed, and stored at −80 °C for protein extraction and quantification. A portion of the liver was instantly fixed in neutral buffered saline (10% NBF) for histological and immunofluorescence analysis.

Liver Histology

Fixation of liver tissue was carried out by immersing in NBF for 24 h. The paraffin-embedded fixed tissue was sectioned with a microtome at a thickness of 4 μm after dehydrating with graded alcohol. Several significant pathological changes were evaluated by using H&E (Hematoxylin and Eosin), MT (Masson's trichrome) staining.

Biochemical Assays

Accu-check Glucometer was used to check the serum glucose level, and ALT, AST, Total cholesterol, Triglycerides, LDL, HDL levels were measured using commercial kits (Auto span, ARKRAY Healthcare Pvt. Ltd, Surat, India) on a microplate reader (Thermo Fisher Scientific).

Insulin Tolerance Test

Insulin tolerance tests were performed at the end of the repeated study. Food was removed from the cages 24 hours before the test. Insulin (0.5 U/Kg of body weight) was administered subcutaneously. Blood glucose levels were checked at 30, 60, and 120 min after insulin administration.

Oral Glucose Tolerance Test

Oral glucose tolerance tests were performed at the end of the repeated study. Food was removed from the cages 12 hours before assays of fasting, fed Blood Glucose Levels and Blood Glucose Tolerance Test. The glucose tolerance test was carried out on mice that had been fasting for 12 h. 40% glucose solution (2 g/kg of body weight) was administered in the mice. Blood was collected from the tail vein 0, 30, 60, and 120 min after glucose administration, and the glucose levels were measured with an Accu-check glucometer.

Analysis of Cytokines by ELISA

Serum was isolated as mentioned above, and the levels of tumor necrosis factor-α (TNF-α), interleukin-6 (IL-6), interleukin 18 (IL–18), and interleukin-1β (IL-1β) were examined using the commercially accessible kit for ELISA according to the manufacturer's instruction and guidelines (R&D Systems, Minneapolis, MN). The same was also measured from HepG2 cell supernatant. FFA treated and MLT treated cells were then incubated with serum-free media for 24 h and then the supernatant was collected.

Hepatic Protein Measurement by Western Blot Analysis

Isolation of total protein from HepG2 cells and Liver tissues were performed using cell lysis buffer and RIPA lysis buffer, respectively, supplemented with protease and phosphatase inhibitor cocktail; proteins have been quantified by BCA Assay kit (Thermo Fisher Scientific). The equal amounts of protein (30 µg of protein/sample) were separated from each sample by 8–15% SDS-PAGE (Bio-Rad, Hercules, USA) and transferred to a PVDF membrane (polyvinylidene difluoride membrane; Millipore, Bedford, USA) by following the wet transfer method. Specific antibodies were taken for the Western blotting analysis. Nonspecific interactions were blocked by 5% BSA. The membranes were incubated with a blocking buffer for 2 h at 37°C. Membrane encompassing the proteins has been exposed to enhanced chemiluminescence plus reagents (Bio-Rad) under Azure Biosystem.

Determination of Hepatic Proteins Expression Using Immunofluorescence

The differentiated HepG2 cells and unstained liver section of all experimental groups have been analyzed through immunofluorescence. Concisely, for the cells, the fixation was performed by 4% PFA, and the cells were blocked by 5% BSA for 1 hour. In the case of tissue, the liver tissues were fixed in NBF, and then tissues were paraffin-embedded and sliced by a microtome. After these sections were deparaffinized and hydrated in graded ethanol, antigen retrieval was performed using a microwave oven, and slides were submerged in a citrate buffer (10 mM, pH 6.0) at 90–95°C for 20 minutes. After antigen retrieval, the sections were blocked with BSA (5%) for 2 h at 37°C. The cells and liver tissue section containing slides were incubated with desired primary antibodies (dilution: 1:250) at 4°C for overnight. The samples were washed with PBS and incubated with secondary antibodies (anti-rabbit/mouse/goat-FITC/phycoerythrin (PE)/Alexa Fluor 647 (AF647)/Alexa Fluor 555 (AF555) /Alexa Fluor 488 (AF488)/CFL 555) for 1 hour each at 37°C. The nucleus was stained with Hoechst 33,342 for 20 minutes. The images were taken by Olympus FV10i Laser Scanning confocal microscope (Olympus Corporation, Tokyo, Japan) and Leica TCS SP8 super-resolution lighting microscope.

Isolation and Culture of Mononuclear Cells (MNCs) or Kupffer Cells

Isolation and culture of hepatic mononuclear cells (MNCs) or Kupffer cells were performed following an established method of in vitro collagenase (0.05%) digestion of liver tissues.[33] In short, liver tissues were minced with scissors. Collagenase solution was added to the liver specimens and was shaken for 15 minutes at 37°C. Next, the liver specimen was filtered through a cell strainer, suspended in Percoll solution (33%) containing heparin, and centrifuged (500 g) for 12 min at room temperature. The pellets were incubated in a red serum cell lysis buffer and then washed thrice in a complete RPMI medium. Nearly 30–35% of mononucleated cells were plastic adherents and these cells were regarded as Kupffer cells. Primary MNC cells were incubated for 48 hours in 6-well plates in triplicate at 37°C in 5% CO2, and the supernatants were collected for cytokine detection through ELISA.

Flow Cytometry

MNCs were stained with FITC-conjugated anti-F4/80 antibody, PE-conjugated anti-CD11b antibody and APC conjugated Pro-IL-1β antibody. Flow cytometry was performed using BD LSR (Fortessa, San Jose, CA, USA).

Primary Hepatocyte Isolation

An established method was followed to isolate primary hepatocytes.[34] Briefly, mice were anesthetized and dissected the abdomen to reveal the portal vein and vena cava. The needle was gently inserted around the vena cava and the perfusion buffer was allowed to perfuse through the liver. Right after that the portal vein was slashed. The perfusion was then replaced with a collagenase solution to digest the liver. After 10 minutes, the liver was taken to a petri dish containing perfusion buffer 2. The lobes were minced by forceps, and the whole solution was filtered through a cell strainer (100 µm), and the cell suspension was transferred into centrifuge tubes. The cell suspension was centrifuged at 50 g for 5 minutes. As parenchymal cell sediments and non-parenchymal dead cells float in the supernatant, the supernatant was discarded. This step was repeated at least thrice. The hepatocytes were then resuspended in complete DMEM media before experiments.

Reactive Oxygen Species Measurement

ROS was measured using fluorescence spectrophotometry, with 2',7'-DCF-DA (2',7'-dichlorofluorescein diacetate) as the probe. DCF-DA freely enters through the membrane, and later on enzymatically cleaved by intracellular esterases to the non-fluorescent DCFH (2',7'-dichlorodihydrofluorescein), which can then be rapidly oxidized to fluorescent DCF in the presence of ROS. Primary hepatocytes were isolated and incubated with 10-μM DCF-DA for 20 min at 37°C in the dark. The supernatant was collected to measure the production of ROS, and the intensity of DCF fluorescence was immediately read in a fluorescence spectrophotometer at 485 nm for excitation and 520 nm for emission.

Ca^{2+} Ion Measurement Using Fluo-3 AM

Intracellular Ca^{2+} was determined by using a flow cytometer. HepG2 cells were collected by trypsinization and centrifuged at 350 g for 5 min and primary hepatocytes were also collected from the mouse as described previously. The cells were incubated in an incomplete medium containing Fluo-3 AM (1 μM) for 30 min at 37°C in the dark. The cells were then centrifuged and the pellets were washed with 1XPBS twice. Finally, the cells were re-suspended in 400 μL of 1XPBS, and the fluorescence intensity was instantly quantified with a flow cytometer. (Excitation wavelength = 488 nm and emission wavelength = 525 nm.)

Docking Study

Recombinant P2X7 (PDB ID: 5U1Y) were taken from the RCSB protein database bank (http://www.rcsb.org), and canonicalSMILES of Melatonin was obtained from PubChem (https://pubchem.ncbi.nlm.nih.gov). Then, the molecular docking score was calculated in mcule using AutodocVina. Nine docking poses were provided and representative images were analyzed using BIOVIA Discovery Studio Visualizer.

Co-Immunoprecipitation Assay

Co-IP is an efficient technique for quantifying protein–protein interaction in cells. Briefly, 600 μg of cellular proteins were labeled using an anti-melatonin antibody (Invitrogen, Catalog # PA5-77490) following overnight incubation at room temperature. The protein-antibody immunoprecipitants were collected by protein A/G plus-agarose (Santa Cruz Biotechnology, USA). After the final wash, the samples were boiled and centrifuged to pellet the agarose beads. Western blot analysis of the P2X7 protein in the supernatant was then conducted. Antigens were visualized using a ChemiDoc imaging system (Azure Biosystems), and data were analyzed using ImageJ software.

Determination of Renal Superoxide Dismutase (SOD) Activity

Using a commercially available kit (Sigma-Aldrich Co.), which underlies the protocol of WST-1 (highly water-soluble tetrazolium salt) reduction method according to the manufacturer's instruction, the activity of SOD was determined.

Determination of Renal Reduced Glutathione (GSH) Level

The tissue lysate was treated with 0.1 mL of TCA (25%), and the resulting precipitate was pelleted by centrifugation at 3900×g for 10 minutes. The free endogenous sulfhydryl was assayed in the reagent-lysate mixture (3 mL), containing 2 mL of 0.5 mM 5,5′-dithiobis-2-nitrobenzoic acid (DTNB) with 1 mL of liver tissue lysate. The reduced GSH reacted with DTNB and formed a yellow-colored complex. Finally, the absorbance was measured at 412 nm.

Statistical Evaluation

All data are presented as the means and standard deviations. All experiments were performed in triplicate; data were randomly collected. We performed a one-way ANOVA (a categorical independent variable), Tukey's post hoc multiple comparisons test was applied to an additional analysis of the differences between groups using GraphPad Prism 8.0 software (GraphPad Software, San Diego, CA, USA). $P < 0.05$ was considered to be significant.

Results

MLT Reversed HFD-Mediated Hepatic Anomalies

Obesity-related pathologies, such as non-alcoholic fatty liver disease (NAFLD), have recently emerged as the most common hepatic disorder. If untreated, NAFLD could transform into cirrhosis and nonalcoholic steatohepatitis (NASH), which is characterized by the presence of chronic inflammation, macrosteatosis, ballooning degeneration, and pericellular fibrosis of hepatocyte.[35] To determine the know-how mechanism of MLT in preventing the NASH as well as to select the optimum dosage of MLT at which maximum activity was achieved, different concentrations of MLT (10, 20, 40, and 80 mg/kg) were given intraperitoneally for 1 month on every alternate day in the beginning. Preliminary experimentation on hepatic toxicity indices (ALT and AST) was performed to evaluate the underlying toxicity of MLT (Supplementary Figure 1). No such enhancement of toxicity indices was found when treated with MLT alone, suggesting the non-toxic potentiality of MLT. In the case of 10 and 20 mg/kg body weight of MLT treatment with HFD, no such changes in physical parameters were observed. In contrast, a slight enhancement of the AST and ALT levels was seen across the control group when treated with 40 and 80 mg/kg. Thus, these two dosages of MLT (10 and 20 mg/kg) were selected for the entire study to evaluate the anti-obesogenic potential (Supplementary Figure 1).

As seen in Table 1, when feeding with HFD for 6 months, the average body weight and liver weight were markedly increased across the control group after the completion of experimentation. MLT (10 and 20 mg/kg) treatment reduced the body weight and relative liver weight as compared to the HFD-fed group, indicating the anti-obesogenic potential. MLT also suppressed the HFD-mediated enhancement of total cholesterol, triglyceride, and LDL cholesterol. Additionally, MLT also repressed the random serum glucose in the obese condition, which indicated the plausible action of glucose utilization (Table 2 and Supplementary Figure 2). Fasting blood glucose level and serum insulin level were measured on the last day of

Table 1 Physiological Parameters of Experimental Mice Groups

	Body Weight (gm)	Liver Weight (gm)	Liver Weight/Body Weight Ratio (%)
NCD	32.800±0.980	1.100±0.376	3.173±0.084
HFD	49.200±1.166$^{\#}$	1.788±0.050$^{\#}$	3.837±0.094$^{\#}$
HFD+MLT D1 (10 mg/kg)	41.600±1.020$^{\#}$	1.418±0.066$^{\#}$	3.409±0.121$^{\#}$
HFD+MLT D2 (20 mg/kg)	38.000±1.095$^{\#}$	1.164±0.042$^{\#}$	3.279±0.121$^{\#}$

Note: P value < 0.0001 = #, P value.

Table 2 Biological Parameters of Experimental Mice Groups

	NCD	HFD	HFD+MLT D1 (10 mg/kg)	HFD+MLT D1 (20 mg/kg)
Blood Glucose (mg/dL)	82.75±3.351	290.5±4.573$^{\#}$	184.25±3.473$^{\#}$	128.5±2.273$^{\#}$
AST (IU/L)	47.908±1.920	154.206±9.750$^{\#}$	92.717±9.628$^{\#}$	58.007±3.601$^{\#}$
ALT (IU/L)	66.638±2.989	164.597±8.176$^{\#}$	102.426±9.152$^{\#}$	68.968±3.603$^{\#}$
AST/ALT ratio	0.719±0.007	0.9365±0.024$^{\#}$	0.904±0.014ns	0.841±0.014$^{\#}$
Triglycerides (mg/dL)	88.207±2.720	110.677±3.324$^{€}$	99.67±2.808ns	86.533±2.932$^{€}$
Total Cholesterol (mg/dL)	160.079±1.038	195.675±0.881$^{\#}$	188.708±1.625$^{€}$	175.252±.7028$^{\#}$
HDL (mg/dL)	64.748±0.185	55.289±.858$^{\#}$	61.927±.405$^{\#}$	64.122±.256$^{\#}$
LDL (mg/dL)	77.303±1.162	118.238±1.066$^{\#}$	106.626±1.642$^{¥}$	93.132±0.971$^{\#}$

Notes: Data are represented as the mean percentage ± SEM (n=3). P value < 0.0001 = #, P value < 0.001 = ¥, P value < 0.01 = €, P value < 0.05 = £.
Abbreviation: ns, non-significant.

MLT treatment. Reciprocal changes have been observed between these two parameters following treatment with MLT. To establish the accuracy of the experimental mice groups and their correlation with glucose homeostasis oral glucose tolerance test (OGTT) and insulin tolerance test (ITT) has been performed and the data suggest significant tolerance of glucose in MLT treated groups. Results from ITT suggest an improved reduction of blood glucose in MLT treated groups compared to the HFD treated mice group (Supplementary Figure 3).

The change in the histopathological architecture of hepatic tissue was also examined to determine the degree of damage. An extensive occurrence of micro/macrovesicular steatosis with lobular inflammation, hepatocyte ballooning degeneration, Mallory's hyaline, and fibrosis was seen in HFD-fed liver. However, MLT treatment significantly reversed the hepatic anomalies. The presence of ballooning degeneration was low in the high dosage of MLT treatment (20 mg/kg) compared to low dosage treatment (10 mg/kg), reflecting that MLT in higher dosage (20 mg/kg) had significant inhibitory activity on lipid droplet accumulation. The histopathology scoring (steatosis score, ballooning degeneration score, inflammatory score, and NAFLD score) also demonstrated the gradation of damage. The HFD fed mice exhibited grade-3 steatosis, whereas MLT+D1 was assigned to grade-2, and MLT+D2 showed the grade-1. Similarly, NAFLD grading depicted that NCD fed mice had stage-0, HFD fed mice showed stage-4 (mixed steatosis with lobular inflammation, hepatocyte degeneration with ballooning, macrovesicular steatosis, Mallory's hyaline and fibrosis), HFD+D1 mice had stage-3 (microvesicular steatosis with lobular inflammation and hepatocyte ballooning) and HFD+ D2 mice had stage-1 (simple steatosis). According to the cumulative damage scoring, HFD fell in grade 3 (severe), HFD+MLT D1 fell in grade 2 (moderate), whereas HFD+MLT D2 fell in stage 1 (mild) (Figure 1).

MLT Reduced HFD-Induced Kupffer Cell Activation

The activation of the Kupffer cell has been considered as one of the causal factors for developing NASH.[36] Reports demonstrated that the recruitment of inflammatory cells into the liver and their subsequent activation contribute to the progression of NASH. To investigate the role of Kupffer cells in the development of proinflammation and to check the MLT in inhibiting the activation, flow cytometric strategies were adopted. The murine phenotype of the Kupffer cell was determined by the presence of dual marker, F4/80 +Ve, and CD11b +Ve. An enhanced population (48.2%) of F4/80 +Ve/CD11b +Ve cells was found in obese liver, indicating the probable activation of Kupffer cells upon HFD treatment (Figure 2B), whereas in MLT treated groups, F4/80 +Ve/CD11b +Ve cells (29.3% and 21.3%) were significantly reduced in a dose-dependent manner (Figure 2B). Further, the HFD group also showed enhanced expression of pro-IL-1β (31.9%), and interestingly, MLT treatment in dual dosage lowered the pro-IL-1β population, respectively, ie, 22.4% in HFD+D1 and 19.4% in HFD+D2. ELISA of IL-1β also supports the finding that MLT treatment lowered the level of IL-1β (Figure 2D). These results signified the underlying mechanism of Kupffer cell-guided modulation of proinflammation during NASH.

MLT Impairs HFD-Mediated Inflammasome Activation

The progression from NAFLD to NASH is becoming the current research area of interest nowadays. The immunological mechanism has been recognized as one of the essential factors for disease progression. NLRP3 inflammasome, a large intercellular multiprotein complex, is of great importance due to its critical role in regulating inflammation, followed by the transformation from NAFLD to NASH.[37,38] In order to determine the mechanism of MLT on NLRP3 inflammasome modulation, the expression of NLRP3 components was studied through immunoblotting and immunofluorescence. As evident from Figure 3A–D, HFD markedly ($p < 0.05$) increased the expression of the sensor molecule of the inflammasome, NLRP3, and the adaptor protein, ASC with respect to the control group. However, MLT inhibited the NLRP3 and ASC activation when compared with the HFD-treated situation, indicating the MLT might play an inhibitory role in regulating inflammasome activation. Additionally, immunofluorescence micrographs depicted that HFD significantly enhanced the NLRP3 and ASC expression throughout the hepatocyte, as observed from the relative fluorescence intensity of NLRP3-CFL555 and ASC-AlexaFluor488. Contrastingly, the enhanced expression was reversed with the treatment of MLT in dual dosage (10 and 20 mg/kg). MLT also reduced the expression of precursor procaspase-1 as well as the proinflammatory cytokines, active IL-1β, and IL-18 significantly ($p < 0.05$) in the HFD-fed situation, suggesting that MLT could repress the proinflammatory burden via the inhibition of inflammasome (Figure 3E–G). Western blot analysis of NLRP3 and ASC proteins in Kupffer cells suggested that a decrease in these two major proteins of inflammasome

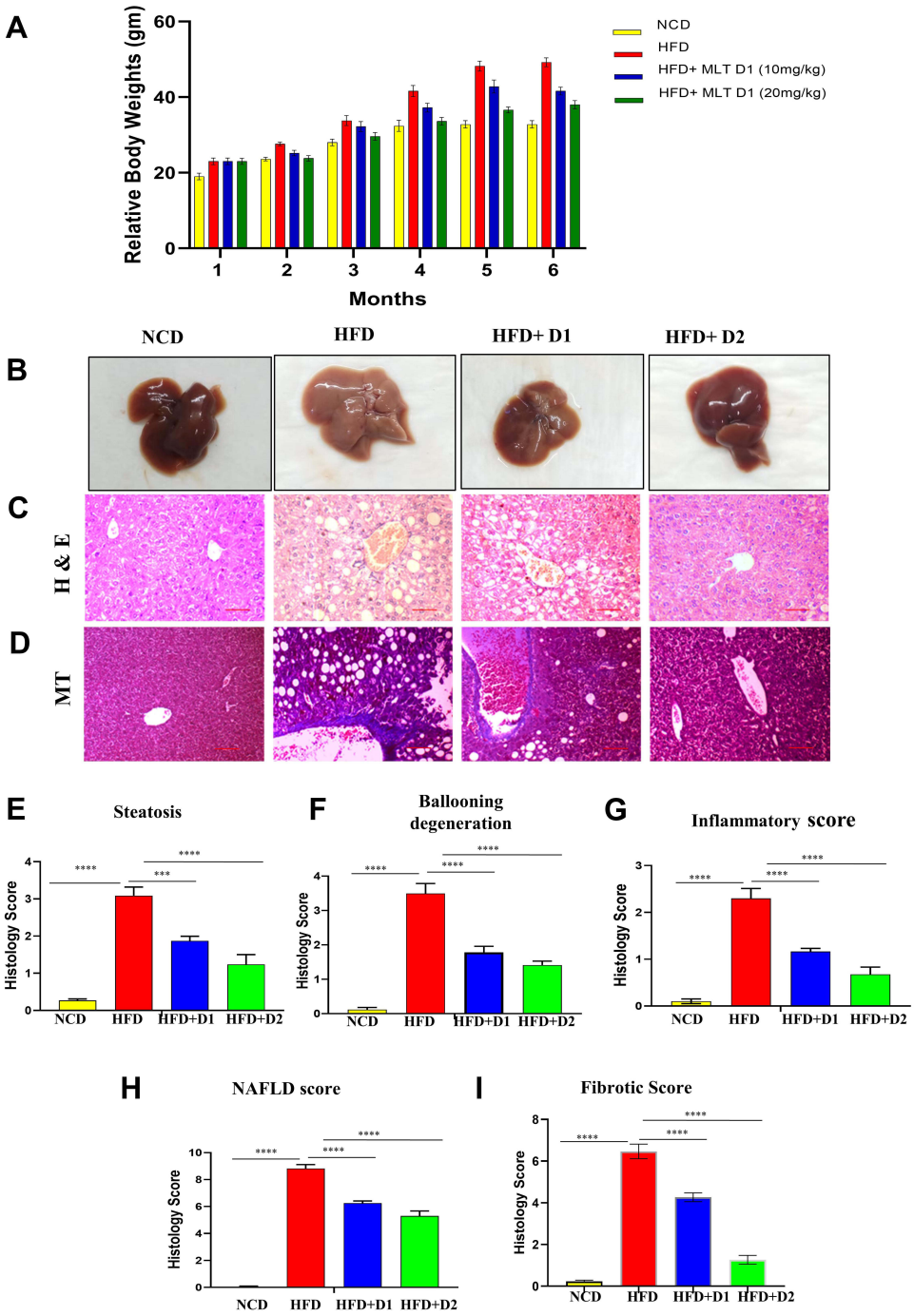

Figure 1 MLT reversed HFD-mediated hepatic anomalies. Male C57BL/6 mice were administered high fat diet (HFD) or a normal control diet (NCD) for 6 months, together with MLT (10mg/kg/day, 20mg/kg/day) for every alternative day. (**A**) Relative body weight changes in different groups. (**B**) Representative images of Liver of different groups, (**C** and **D**) cross-sections of Liver with HE and MT staining in the different groups. Scale bars = 100 μm. (**E–I**) Histology score of different groups, The values indicate the mean ± SEM (n=3) ***P<0.001, ****P<0.0001.

complex has shown significant reduction in their level in MLT treated groups with respect to the HFD fed group (Supplementary Figure 4).

Another set of in vitro experiments was carried out to confirm the mechanistic crosstalk of MLT-guided inflammasome inhibition. The cytotoxicity of MLT was examined by MTT assay in HepG2 cells. The bar graph shows the percentage of death of cells upon MLT treatment in different dosages (50, 100, 200, 400, 800, 1600 μM). As shown in the

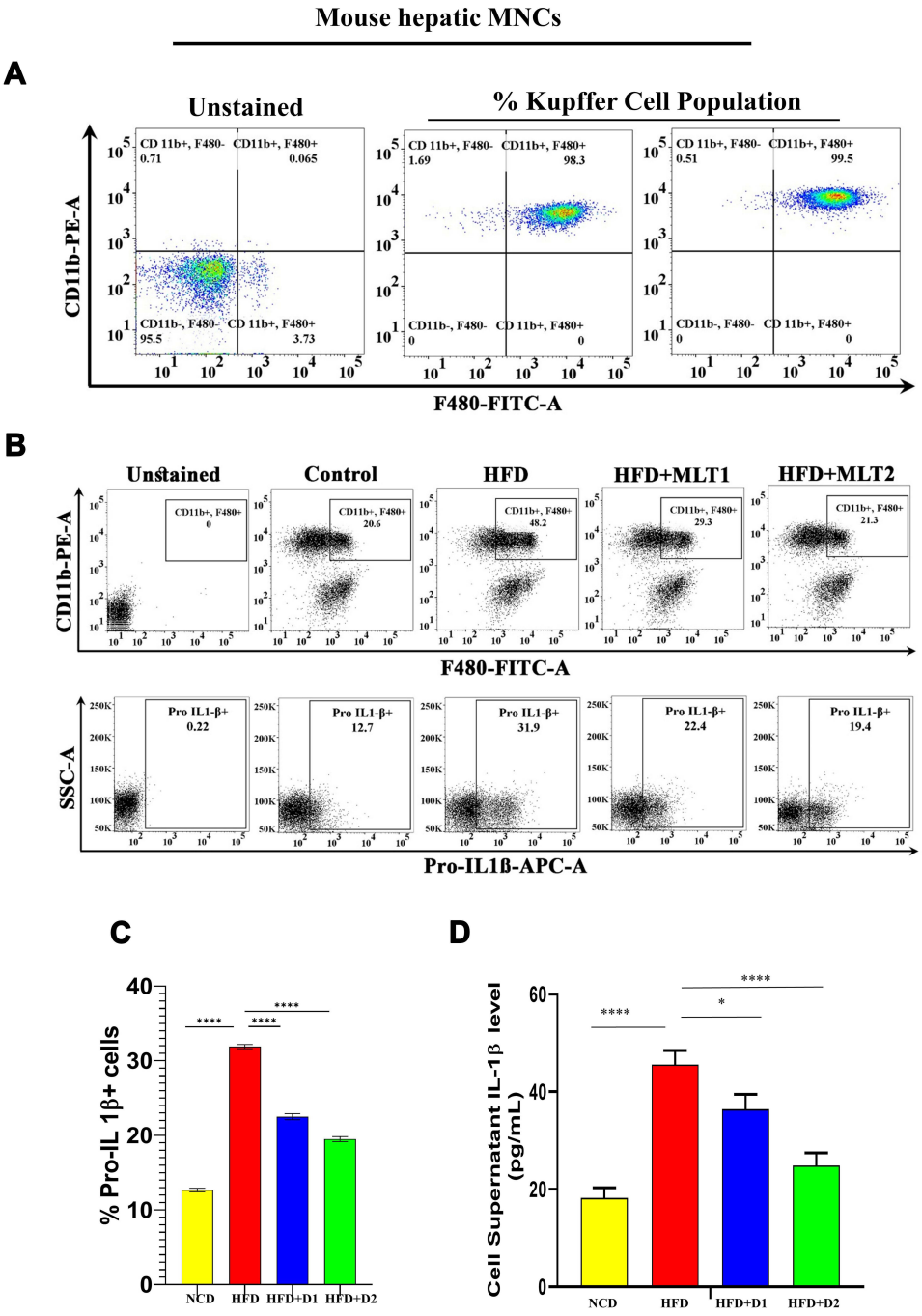

Figure 2 MLT reduced HFD-induced Kupffer cell activation. (**A**) Characterization of Kupffer cells by flow cytometric analysis using F480-FITC and CD11b-PE dual staining (**B**) Change of the activated Kupffer cells population in HFD and MLT treated groups and simultaneously Pro-IL 1β level also checked by flow cytometry using Pro-IL-1β-APC. (**C**) Bar graph of Pro-IL1β population observed from Kupffer cells (**D**) Kupffer cell were isolated from the mice liver and IL-1β was measured by ELISA from the cell supernatant. The values indicate the mean ± SEM (n=3). *$p < 0.05$, ****P<0.0001.

figure, the MLT exerts a minimal amount of cell death in 50–100 µM, ie, less than 5%; 50 µM dose was selected for further study (Supplementary Figure 5).

As evident from Figure 3I MLT suppressed PA/OA-stimulated NLRP3 and ASC expression. On the other hand, in the concurrent treatment with the selective inhibitor of NLRP3 (Glyburide) and MLT, the expression of NLRP3 and ASC was diminished markedly ($p < 0.05$) (Figure 3K–L). The level of secreting pro-inflammatory cytokines, IL-1β and IL-18

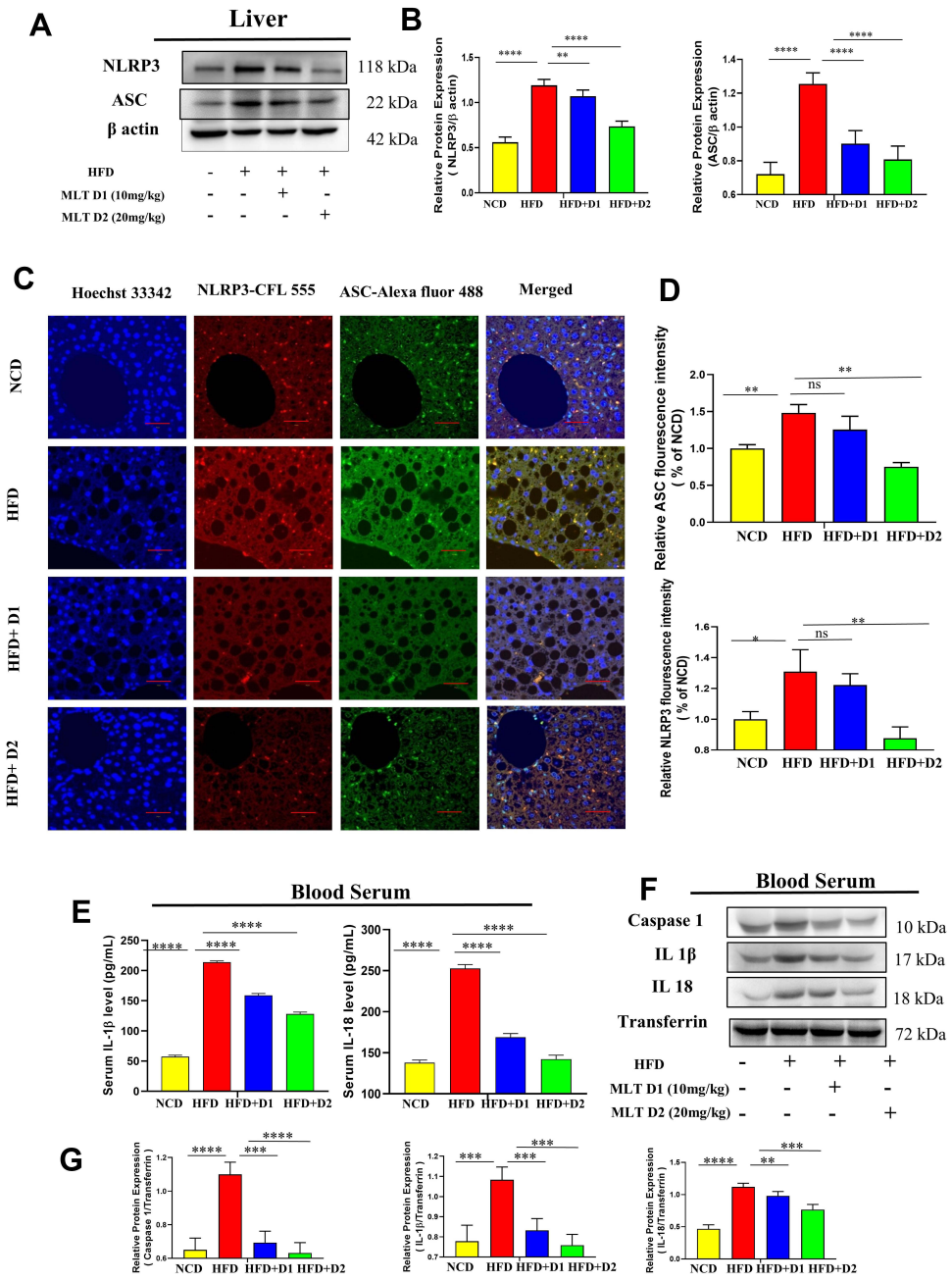

Figure 3 Continue.

in cell supernatant was also suppressed dramatically ($p < 0.05$) (Figure 3H), suggesting that MLT could reduce the pro-inflammatory burden through the inhibition of NLRP3/ASC/Procaspase 1-mediated pathway.

MLT Inhibited HFD-Induced TLR4-Guided NF-κB Activation

TLR4, the pattern recognition receptor (PRR), is one of the essential contributing factors for the development of the proinflammatory condition. Fatty acid could trigger the TLR4 activation in the obese condition which influences the inflammasome assembly through the upregulation of redox-sensitive transcription factor, NF-κB. NF-κB has long been regarded as prototypical inflammatory pathways, based on the activation of a plethora of cytokines.[39,40] To investigate the role of MLT in TLR4-mediated inflammasome activation, the expression pattern of TLR4 along with the phospho-NF-κB (p-NF-κB) and total form NF-κB were checked through immunoblot analysis. MLT treatment in dual dosage (10 and

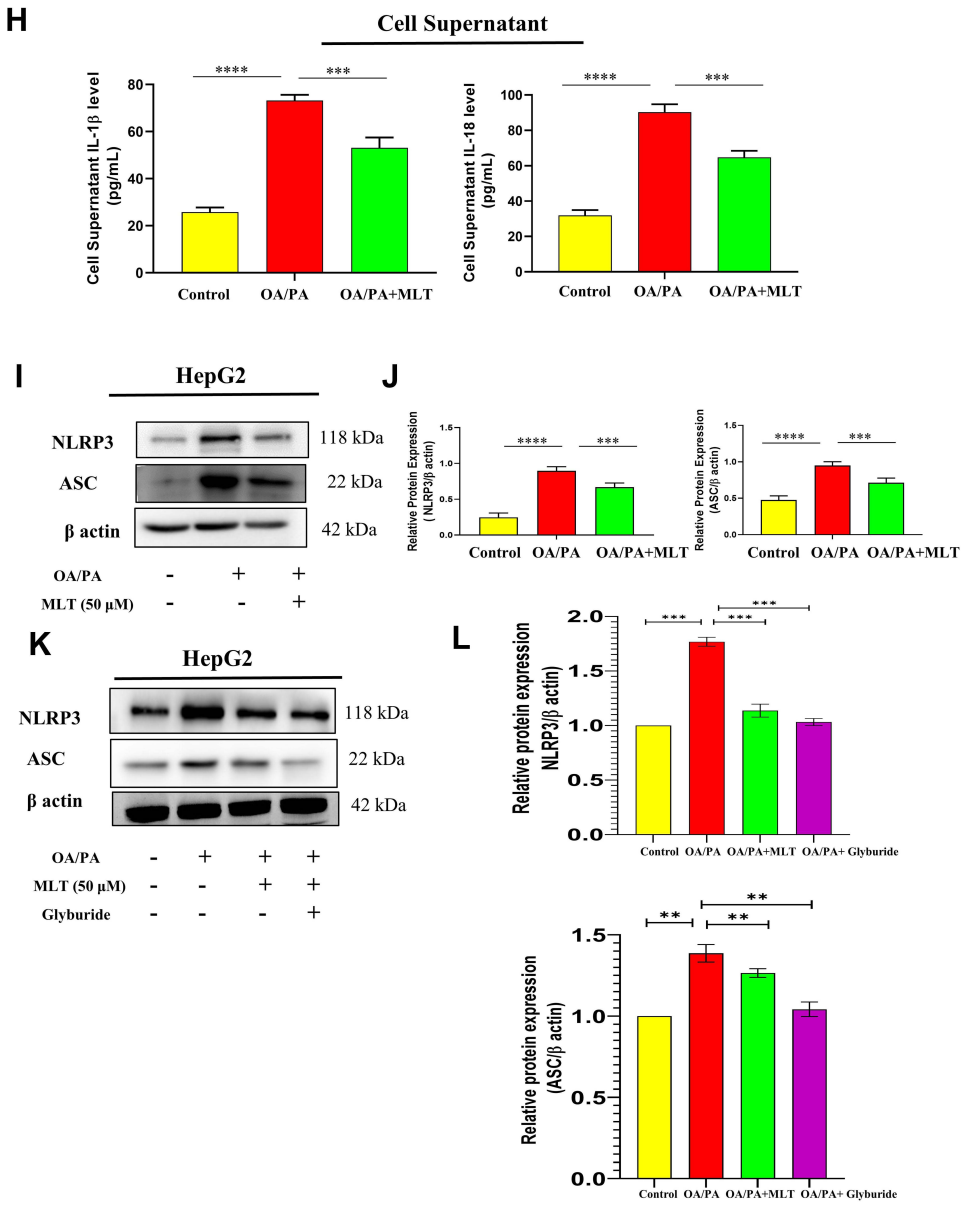

Figure 3 MLT impairs HFD-mediated inflammasome activation. (**A**) Western blot analysis of inflammasome assembly protein NLRP3 and ASC from the liver of different mice groups. (**B**) The bar graph showed the quantification of NLRP3/β actin and ASC /β actin, respectively. (**C**) Representative immunofluorescent images showed NLRP3 and ASC expression in mouse liver depending on the different treatments. Scale bar = 50 μm. (**D**) The bar graph represents quantification of the fluorescence intensity of NLRP3 and ASC shown in the different groups. (**E**) level of IL-1β and IL-18 was analyzed by ELISA from different mice groups. (**F**) Western blot analysis of pro-inflammatory cytokines (Caspase 1, IL-1β, and IL-18) in the serum of different groups. (**G**) The bar graph showed the quantification of Caspase 1/Transferrin, IL-1β /Transferrin, and IL-18/ Transferrin, respectively. (**H**) ELISA of IL-1β and IL-18 in cell supernatant of OA/PA administered HepG2 cells, with or without MLT (**I**) Western blot analysis of NLRP3 and ASC in the OA/PA administered HepG2 cells, with or without MLT. (**J**) The bar graph showed the quantification of NLRP3/β actin and ASC /β, respectively in FFA treated HepG2 cell lysates. (**K**) Glyburide was treated with OA/PA in a different set of the experiment as a positive control and NLRP3 protein expression is shown by Western blot analysis. (**L**) The bar graph represents the relative protein expression of NLRP3/β actin. The values indicate the mean ± SEM (n=3), *$p < 0.05$, **P< 0.01, ***P<0.001, ****P<0.0001.

Abbreviation: ns, non-significant.

20 mg/kg) suppressed the expression of TLR4 as well as p-NF-κB in HFD fed liver. Figure 4B–E revealed an aggravated expression of TLR4 and p-NF-κB in HFD fed hepatic tissue. Dramatically, the relative fluorescence intensity of TLR4-AF488 and p-NF-κB-AF647 was found to be low with the treatment of MLT. The level of proinflammatory cytokines TNF-α and IL-6 was also increased in obese conditions but these indices reduced significantly with the treatment of MLT (Figure 4A), suggesting that MLT could ease the mechanistic crosstalk between TLR4 and pro-inflammatory signaling

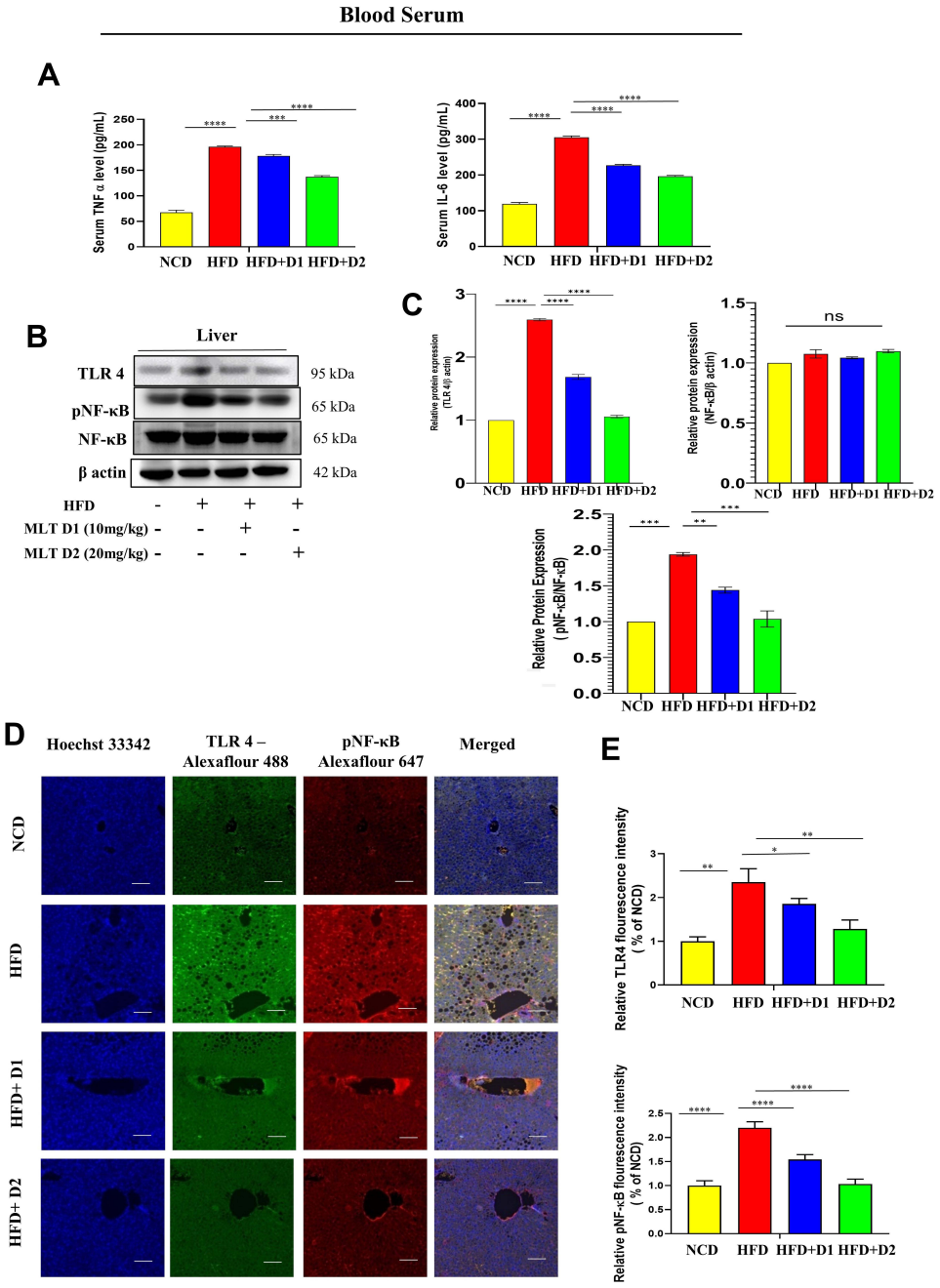

Figure 4 Continue.

pathway. In vitro experimentation was also carried out to verify the levels of TLR4 and p-NF-κB; the Western blot analysis supports the finding of in-vivo experiments (Figure 4F–H).

MLT Suppressed HFD-Induced P2X7 Receptor Activation and Intracellular Ca^{2+}

A growing body of evidence reported that HFD-induced hepatocellular damage causes the release of several damage-associated molecular patterns (DAMP), NAD, and ATP, which trigger the activation of the P2X7 receptor. On the other hand, the enhanced expression of the P2X7 plays an essential role in the regulation of calcium homeostasis, followed by the activation of inflammatory pathways. Intracellular Ca^{2+} is one of the essential factors for the assembly of inflammasome components which is also required for the spontaneous NLRP3 activation.[41–43] To delineate the role of MLT on P2X7

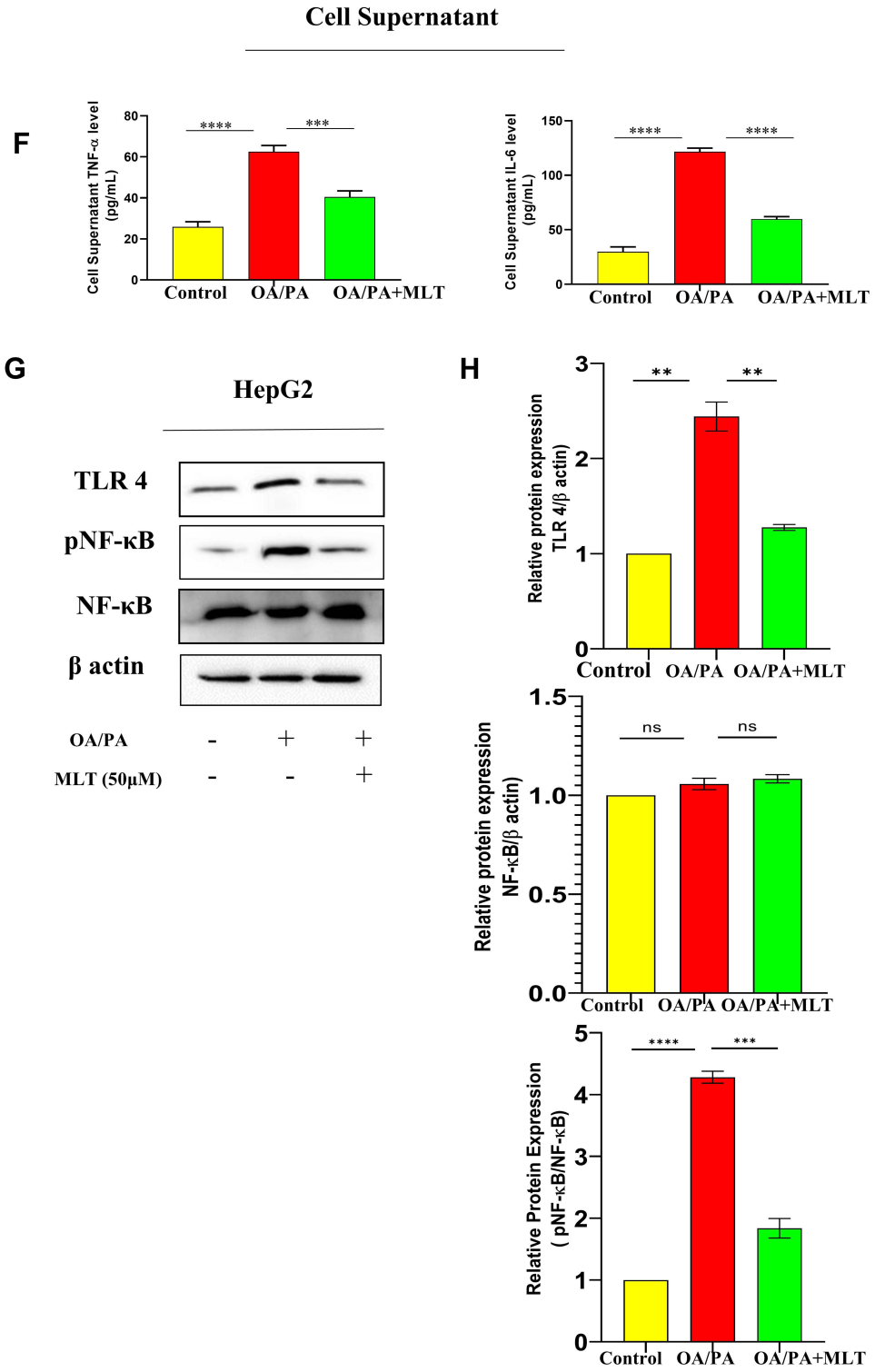

Figure 4 MLT inhibited HFD-induced TLR4-guided NF-κB activation. (**A**) Pro-inflammatory cytokines, such as TNF-α and IL-6 were analyzed from serum by ELISA from different mice groups. (**B**) Western blot analysis of inflammatory proteins (TLR 4, pNF-κB) in the liver of different groups. (**C**) The bar graph showed the quantification of TLR 4/β actin and pNF-κB/NF-κB, respectively. (**D**) Representative immunofluorescent images showed TLR 4, pNF-κB expression in mouse liver depending on the different treatments. Scale bar = 50 μm. (**E**) The bar graph represents the quantification of the fluorescence intensity of TLR 4 and pNF-κBshown in the different groups. (**F**) ELISA of TNF-α and IL-6 in cell supernatant of OA/PA administered HepG2 cells, with or without MLT. (**G**) Western blot analysis of inflammatory proteins (TLR 4, pNF-κB) in the HepG2 cell lysate of different groups. (**H**) The bar graph exhibits relative protein expression of TLR 4/β actin and p-NF-κB/ NF-κB. The values indicate the mean ± SEM (n=3), *p < 0.05, **P< 0.01, ***P<0.001, ****P<0.0001.

Abbreviation: ns, non-significant.

receptor modulation, as well as the intracellular Ca^{2+} mobilization in HFD-induced state, immunoblot and immunofluorescence study, was conducted in both in vivo and in vitro experimental conditions. Enhanced expression of the P2X7 was found upon HFD treatment. Contrastingly, MLT treatment in dual dosage (10 and 20 mg/kg) markedly decreased the expression towards normalcy (Figure 5A and B). Figure 5C and D depicted that the relative P2X7-AF647 intensity was enhanced in the HFD-induced condition. However, the MLT treatment (10 and 20 mg/kg) reduced the AF647 fluorescence intensity compared to the NCD. To confirm the enhancement of P2X7 expression in obese liver and to support the hypothesis, an in vitro experimentation was also carried out. PA/OA treatment augmented the P2X7 receptor activation in HepG2 cells, whereas this activation was significantly diminished with the treatment of MLT (50μM), indicating the inhibitory role of MLT on P2X7 receptor activation (Figure 5F and G). Another set of in vitro experimentation was also

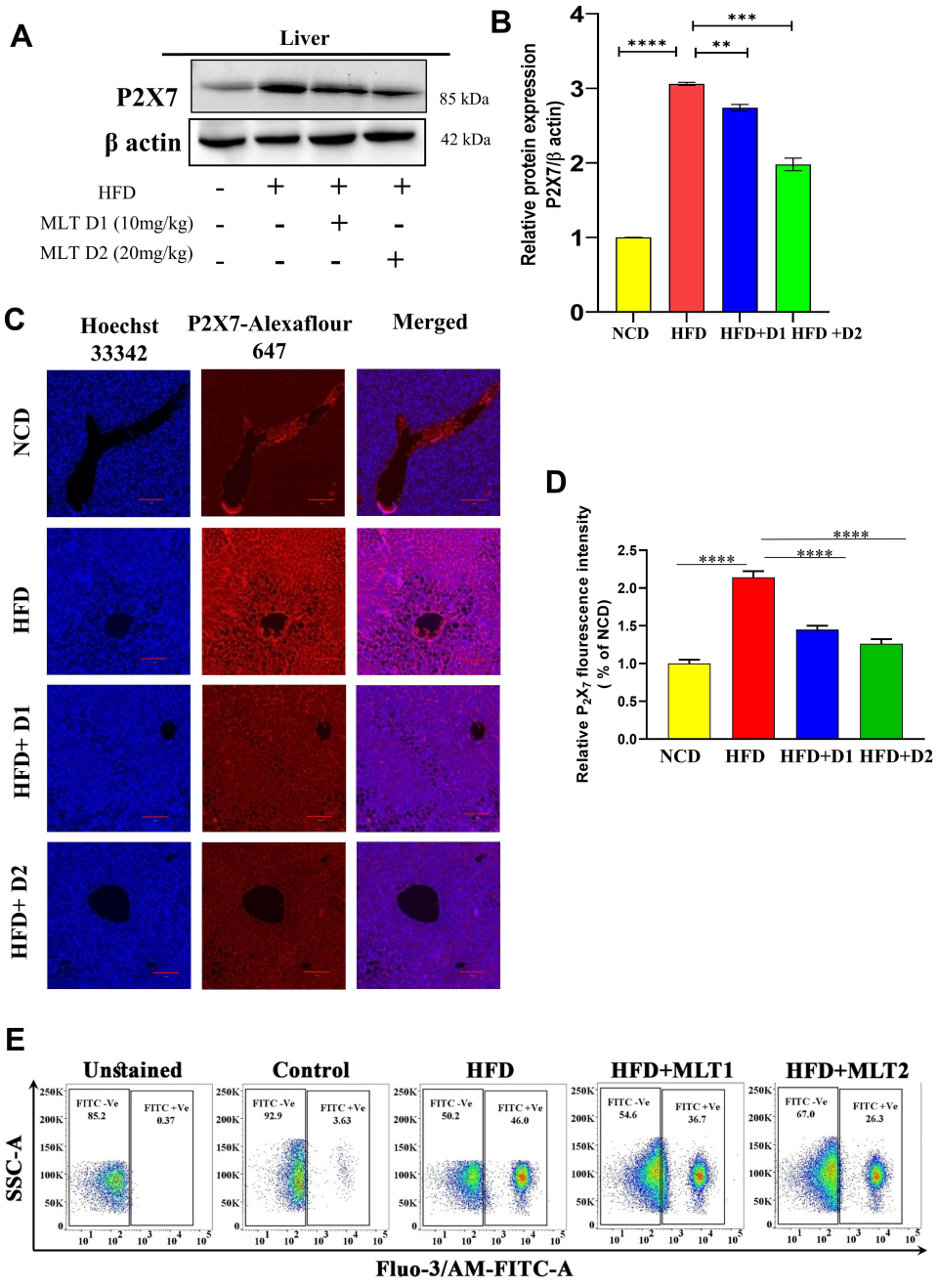

Figure 5 Continue.

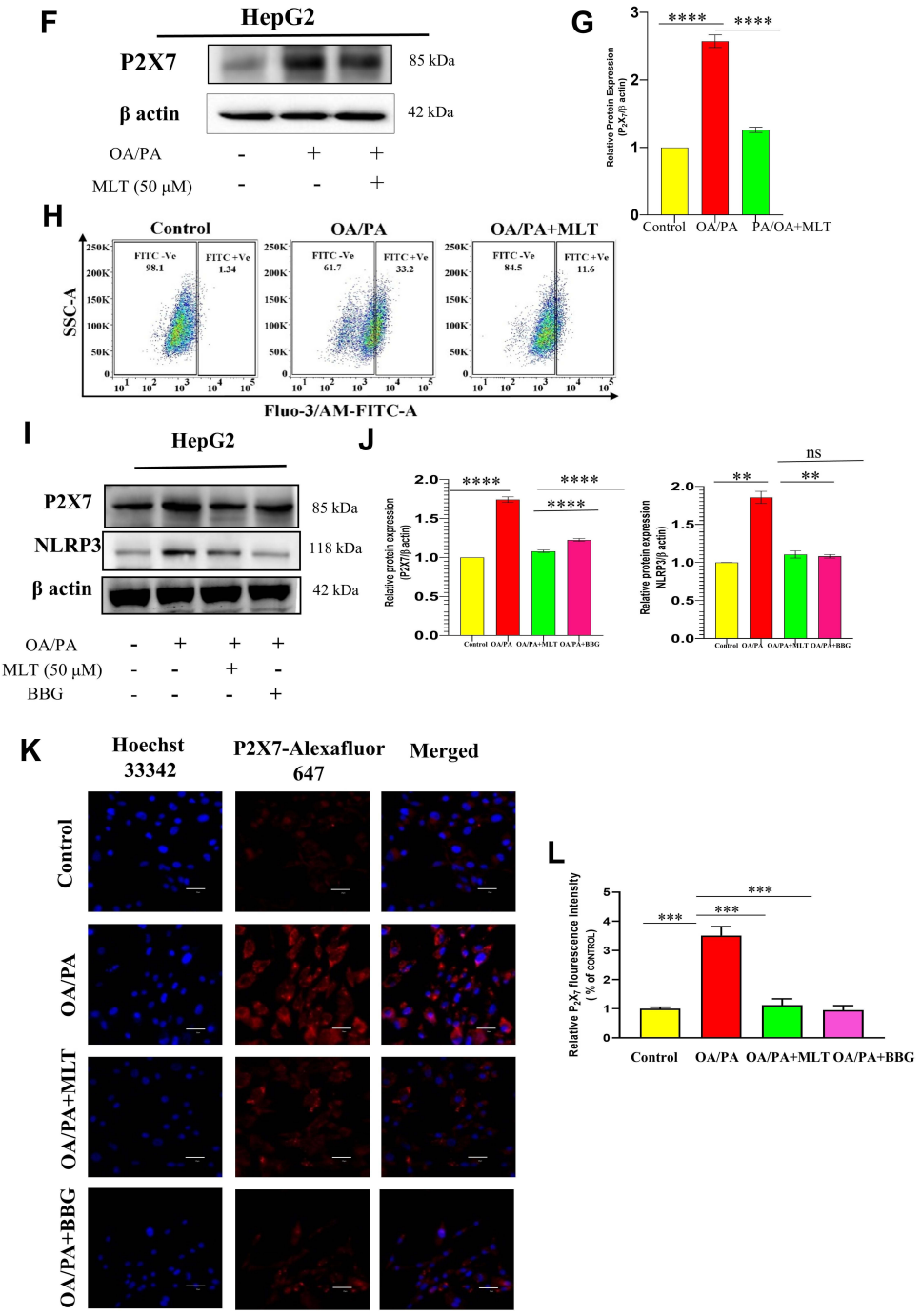

Figure 5 MLT suppressed HFD-induced P2X7 receptor activation and intercellular Ca^{2+} level. (**A**) Western blot analysis of P2X7 protein from the liver of different mice groups, (**B**) The bar graph represents the relative protein expression of P2X7/β actin. (**C**) The immunofluorescent image represents the P2X7 protein expression in the liver of different mice groups, Scale bar = 50 μm. (**D**) The bar graph shows the relative fluorescence intensity of P2X7. (**E**) This data represents intracellular Ca^{2+} ions in the primary liver cells of different mice groups. (**F**) Western blot analysis of P2X7 protein from HepG2 cell lysates administered with OA/PA, with or without MLT. (**G**) The bar graph represents the relative protein expression of P2X7/β actin. (**H**) The data represents in-vitro intracellular Ca^{2+} ion levels. (**I**) the HepG2 cells were treated with known P2X7 inhibitor brilliant blue G (BBG) along with OA/OA and MLT, the Western blot analysis shows P2X7 and NLRP3 protein expression. (**J**) The bar graph exhibits relative protein expression of P2X7/β actin and NLRP3/β actin. (**K**) The immunofluorescent image depicts P2X7 protein expression in different groups (Control, OA//PA, OA/PA +MLT, OA/PA+BBG), Scale bar = 20 μm. (**L**) The bar graph represents the relative expression of P2X7. The values indicate the mean ± SEM (n=3), **P< 0.01, ***P<0.001, ****P<0.0001.

Abbreviation: ns, non-significant.

carried out to determine the apparent correlation between the activation of P2X7 and NLRP3. A selective antagonist of P2X7, brilliant blue G (BBG)-treatment reduced the activation of PA/OA-induced P2X7 in HepG2 cells, which also inhibited the NLRP3 activation, suggesting that MLT could regulate inflammasome through P2X7 receptor inhibition (Figure 5I and J). The immunofluorescence micrograph also validated the observed results of immunoblot analysis (Figure 5K). Flow cytometry analysis showed an increment of intracellular Ca^{2+} upon both HFD and PA/OA treatment, indicating the fact that NASH could trigger the assembly of inflammasome components via the cytosolic Ca^{2+} burden (Figure 5E and H). Interestingly, MLT-treatment inhibited the intracellular Ca^{2+} level in both in vivo and in vitro experimental conditions as observed in the reduction of Fluo-3/AM +Ve cells (FITC +Ve). These results suggested that MLT could regulate P2X7 activation, which limits the intracellular Ca^{2+}-driven NLRP3 activation.

MLT Inhibited HFD-Induced iROS Generation

Several pieces of evidence pointed out the involvement of intercellular reactive oxygen species (ROS) in the progression of NASH.[44–46] Alteration of lipid metabolism in NASH led to hepatic lipid accumulation and mitochondrial dysfunction. Mitochondrial malfunction, as well as the imbalance of pro-oxidant and antioxidant ratio, triggers the generation of ROS. On the other hand, ROS may play an essential role in activating the NLRP3 inflammasome. To elucidate the role of ROS in triggering the NLRP3 activation as well as to assess the scavenging activity of MLT, a flow cytometric analysis was adopted. An augmented level iROS was observed in the HFD-treated condition when compared with the control (Figure 6A and B). Contrastingly, the enhancement was gradually reduced with the treatment of MLT in dual dosage (10 and 20 mg/kg), suggesting the modulatory potential of MLT as a ROS scavenger (Figure 6A).

MLT Suppressed HFD-Induced Nrf2 and NOX Activation

A growing body of evidence demonstrated a correlation between the P2X7 receptor and NOX activation. On the other hand, P2X7 receptor activation could generate ROS through NOX activation. Hence, HFD-induced NOX activation might play an important role in ROS generation. NOX, a membrane-bound oxidase, involves ROS production through a redox reaction with molecular oxygen and NADPH. To evaluate the modulatory role of MLT on NOX expression, immunoblot analysis was carried out. The figure depicted a marked enhancement of NOX expression upon HFD treatment. Interestingly, MLT treatment with dual dosage (10 and 20 mg/kg) suppressed the NOX activation in HFD-treated hepatic tissue (Figure 6C and D), along with this Nrf2 protein expression also increased in the same (Figure 6C and D). Activity of superoxide dismutase (SOD) reduced glutathione (GSH) was measured using the liver lysates of experimental mice groups and the results indicate substantial increase in both enzymes level in MLT treated groups compared to HFD groups (Supplementary Figure 6). Thus, this indicates the plausible mechanism of MLT-mediated inhibition of ROS through NOX-dependent way.

MLT Interacted with the P2X7 Receptor

P2X7 receptor, a ligand-gated cationic channel, plays a vital role in the regulation of proinflammatory mediators. Numerous studies demonstrated that ATP-directed receptor activation could trigger the overstimulation of the NLRP3 inflammasome.[18,47] To determine the possible interaction as well as the potential role of MLT in inhibiting the P2X7 receptor, followed by the inhibition of NLRP3, a molecular docking approach was adopted, establishing the functional correlation between experimental studies with bioinformatics. The computational docking data predicted the MLT bound to the P2X7 receptor through a conventional hydrogen bond, Van der Waals forces, and hydrophobic interaction. The results also demonstrated that MLT tightly bound to ATP binding cassette of P2X7 receptor with the GLN116, TRP167, ARG294, ARG307, and ALA296 at a distance of 2.008 Å, 2.428 Å, 2.084 Å, 2.260 Å, and 3.903 Å, respectively (Figure 7). The relative binding affinity of −8.4 kcal/mol suggested the strongest affinity towards the P2X7 receptor, which further corroborated the previous experimental evidence. The melatonin treatment in the treatment groups (HFD +MLT D1 and HFD+MLT D2) shows that MLT interacts with P2X7 receptor, whereas in the control group and HFD fed group MLT is absent and thus this reflects no interaction with the P2X7 receptor (Supplementary Figure 7).

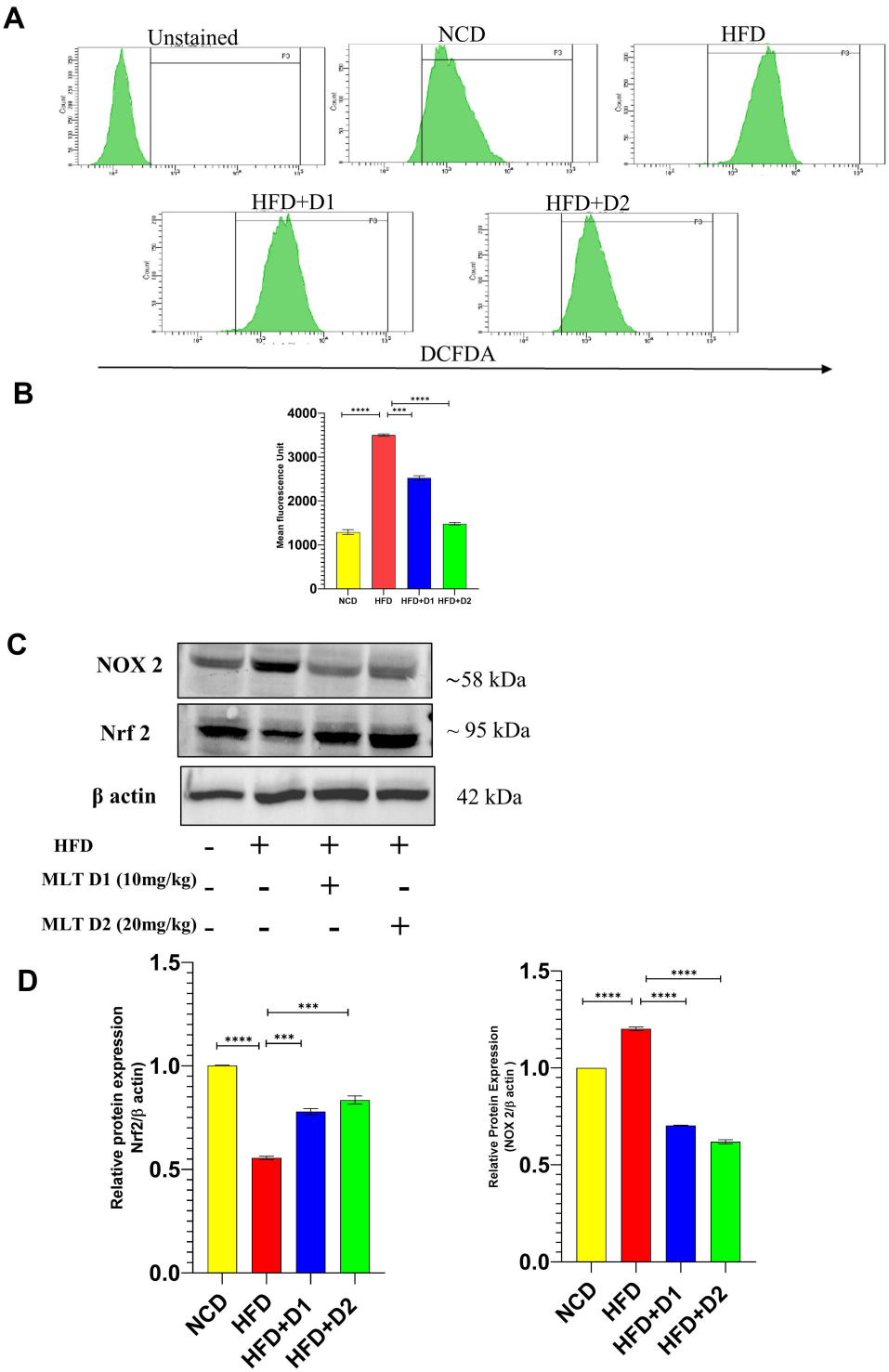

Figure 6 MLT inhibited HFD-induced iROS generation and suppressed NOX activation. (**A** and **B**) Flow cytometric analysis of intracellular ROS and bar graph of mean fluorescence unit of iROS generation, (**C**) Western blot analysis of NOX-2 and Nrf2 protein, and (**D**) the bar graph exhibits relative protein expression of NOX 2/ and Nrf2/ β actin. The values indicate the mean ± SEM (n=3). ***P<0.001, ****P<0.0001.

MLT Inhibited HFD-Mediated Hepatic Fibrosis Through MMP Regulation

Liver fibrosis is a common pathologic consequence of NASH and NAFLD. One of the most important pathological features of liver fibrosis is the increased expression of collagen and structural glycoprotein accumulation that leads to the formation of the extracellular matrix (ECM). Collagen is degraded by matrix metalloproteinase (MMP) which together

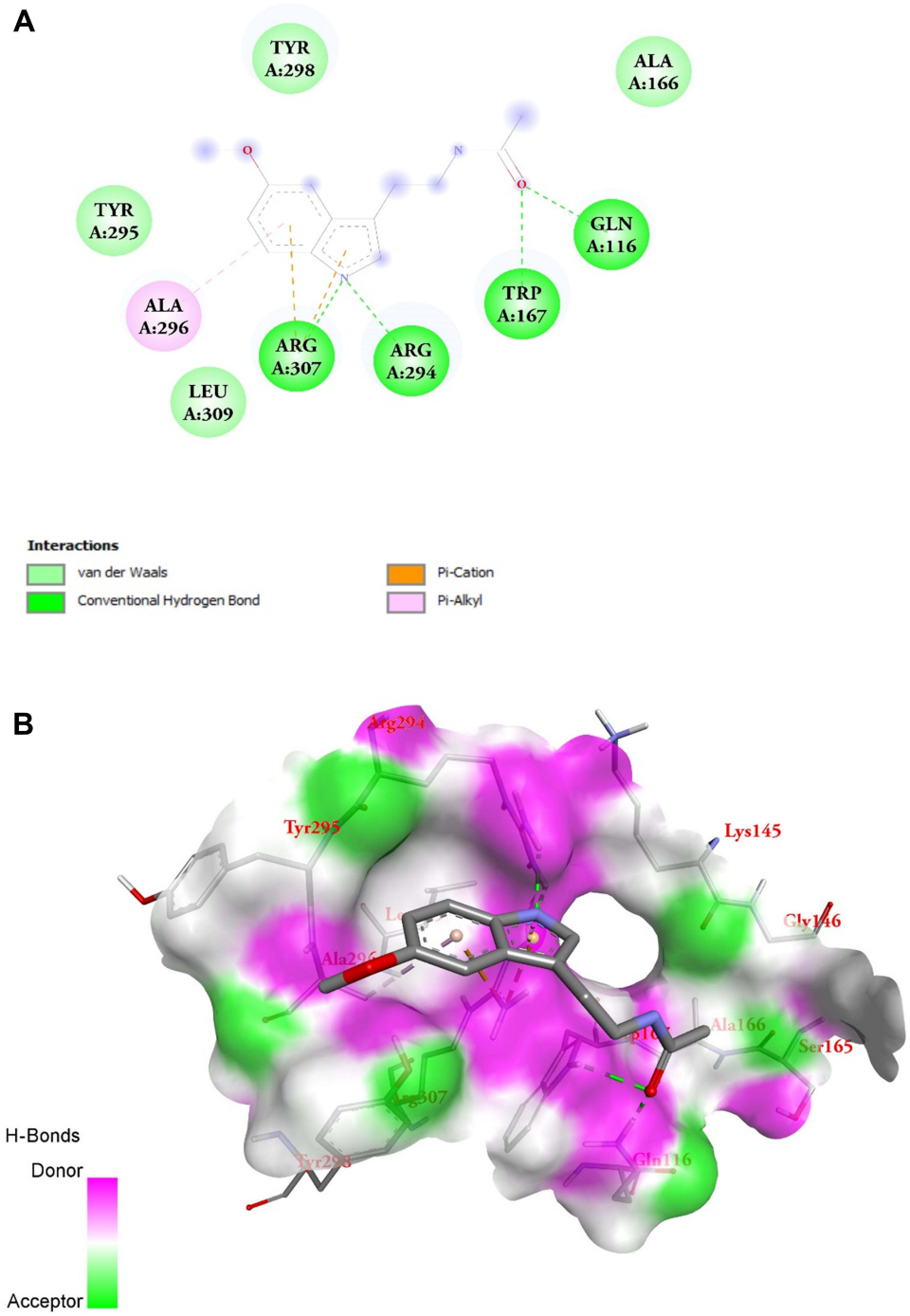

Figure 7 MLT interacted with the P2X7 receptor. (**A** and **B**) 2D and 3D image of molecular interaction study of MLT and P2X7.

with its inhibitor, tissue inhibitor of metalloproteinase (TIMP), is associated with hepatic fibrogenesis. Reports also suggested that NF-κB has been demonstrated to upregulate the MMP2 and 9 by binding to its promoter sequence. Hence, to evaluate the role of MLT in inhibiting hepatic fibrosis, the expression patterns of MMP2, MMP9 and TIMP were checked through immunoblot analysis. Western blot analysis revealed an enhanced expression of MMP2 and MMP9 upon HFD treatment, whereas the expression of TIMP was low in HFD treated conditions, indicating the plausible involvement of matrix metalloproteinase in HFD-induced hepatic fibrosis. The observed expressions were reversed while

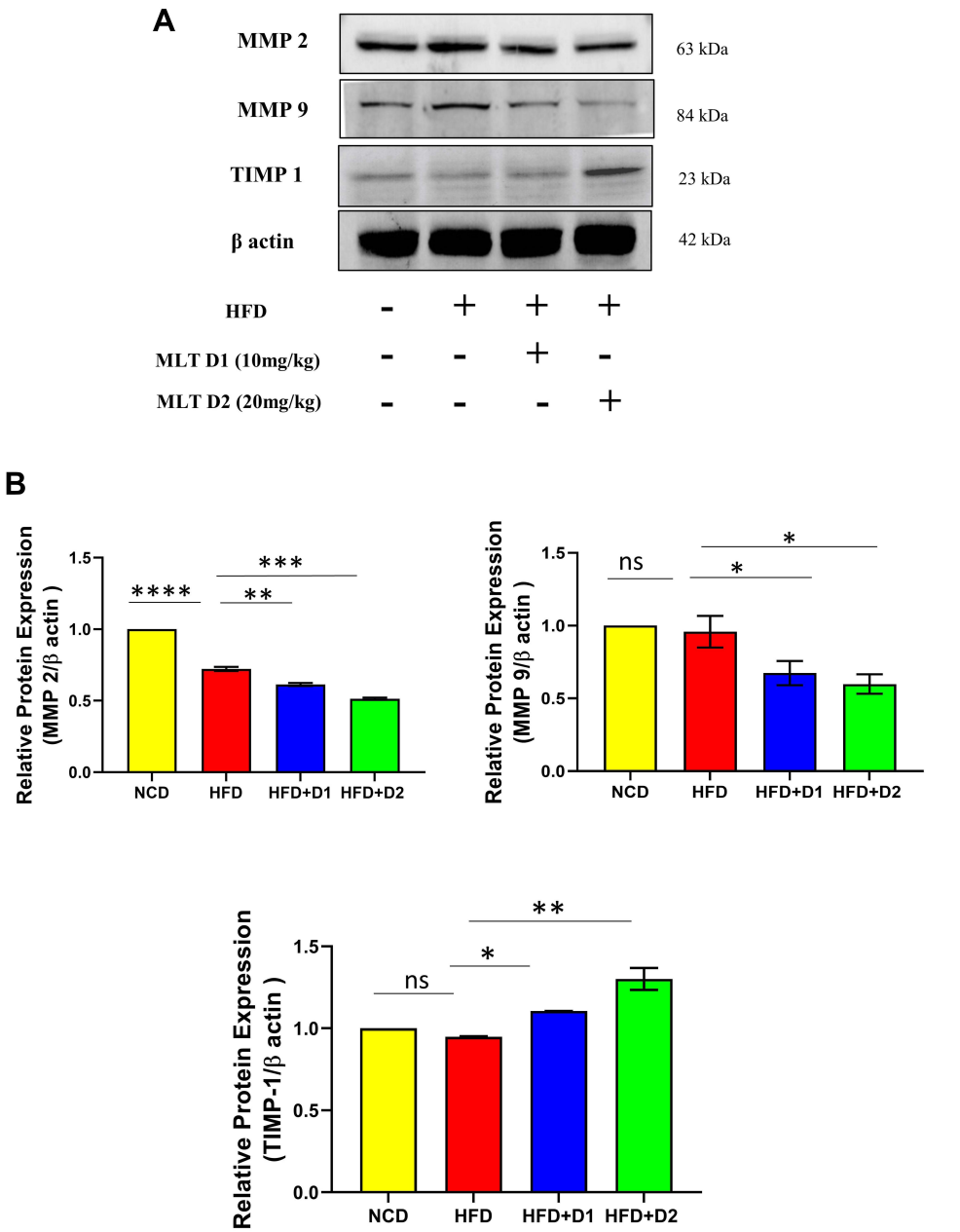

Figure 8 MLT inhibited HFD-mediated hepatic fibrosis through MMP regulation. (**A**) Western blot analysis of MMP2, MMP9, and TIMP 1 protein, (**B**) The bar graph showed the quantification of MMP 2/β actin, MMP 9/β actin, and TIMP 1/β actin, respectively. The values indicate the mean ± SEM (n=3), *p < 0.05, **P< 0.01, ***P<0.001, ****P<0.0001.

Abbreviation: ns, non-significant.

treating with MLT (10 and 20 mg/kg), suggesting that MLT could inhibit liver fibrosis through the modulation of MMP (Figure 8).

Discussion

Melatonin is a lipophilic and hydrophilic indoleamine with various physiological functions. The roles of MT in various liver pathologies have been broadly studied, and it is assumed that oxidative stress and lipid peroxidation are the vital causing factors of almost all conditions compromising liver function, including nonalcoholic fatty liver disease (NAFLD), nonalcoholic steatohepatitis (NASH), diabetes, liver fibrosis, and cirrhosis. NAFLD is defined as a large spectrum of diseases that results from hepatic fat deposition (>5% of liver weight), that further results in hepatic steatosis

(HS, only fact deposition); nonalcoholic steatohepatitis (NASH) that is considered steatosis with inflammation, hepatocyte ballooning and moderate fibrosis; and the progression from NASH to cirrhosis and malignant hepatoma.[38,48] The abundant usage of Melatonin as a substitution therapy for the treatment of different disorders, including liver diseases and injuries, has extended enormously.[49] MLT prevents NLRP3 inflammasome activation by inhibiting or activating several proteins and pathways. NF-κB is a key regulator of the priming phase of NLRP3 inflammasome activation. Melatonin prevents NLRP3 inflammasome activation by inhibiting NF-κB signaling in sepsis.[50]

The present study explored that the P2X7 and NLRP3 inflammasome is a target of the action of MLT in vivo and in vitro experimental model of NASH, providing evidence for a novel mechanism underlying the potent anti-inflammatory activity of MLT. Numerous studies have validated that MLT treatment has effects on inflammation, fat deposition, and energy metabolism and can also improve dyslipidemia.[51–53] The current experimental results showed that MLT (10, 20 mg/kg) significantly reduced NASH in HFD fed mice. In this mouse NASH model, the administration of MLT was effective in alleviating the course of NASH. More precisely, MLT showed a strong tendency to attenuate liver steatosis and to restrict the rise of liver weight and aminotransferases. By contrast, mice on HFD without melatonin showed significantly higher liver weight, liver weight over body weight ratio, aminotransferases, and higher TC, TG, LDL, and HDL (Tables 1–2 and Figure 1).

These results are in keeping with previous studies indicating a hepatoprotective effect of melatonin in rat models of diet-induced NAFLD. These findings are consistent with the reports of Tahan et al, 2009 that indicated MLT showed protective effects on the methionine-choline diet stimulated NASH in rats.[28] However, mechanistic aspects of the amelioration of NASH in the HFD induced NASH model are not well explored.

NLPRP3 inflammasome activation in NASH plays a pivotal role in disease progression through the propagation of inflammation and induction of pyroptosis that eventually causes liver cirrhosis.[54] However, our report first shows that melatonin suppresses NASH by impairing NLRP3 activation via P2X7 receptor inactivation in HFD fed C57BL/6 mice. This P2X7 mediated activation of NLRP3 may be the "Third hit" among multiple hits that primes to NASH from NAFLD. This NLRP3 inactivation is observed in the HFD-induced NASH model and FFA (Oleic acid/Palmitic acid) treated HepG2 cells (Figure 3). Immunoblot analysis of NLRP3 and its adaptor protein ASC from the lysate of FFA treated HepG2 cells and liver tissue of NASH model strongly correlates with the immunohistochemistry of liver tissue section. Suppression of NLRP3 activation by MLT was further confirmed by analysis of its downstream factors, such as active Caspase-1, IL-1β, and IL-18. MLT treatment lowered these downstream molecules as seen in the serum of the NASH model and the supernatant of FFA treated HepG2 cells (Figure 3). Also, several pro-IL-1β producing hepatic Kupffer cells were significantly lowered following MLT treatment, which is another evidence of inflammasome inhibition (Figure 2). Impairment of NLRP3 activation by MLT has been reported in several other inflammations associated with disease models like COPD, brain injury, lupus nephritis, and hypertension[55–59] These findings support our observation on attenuation of the NLRP3 inflammasome by MLT in diet-induced murine NASH.

Growing pieces of evidence suggest that MLT suppresses the inflammatory mediators TNF-α, IL-6, and NF-κB probably through attenuation of TLR4 as observed in many other inflammatory diseases.[60] Consistently, it was found that MLT lowers the inflammatory load by inhibiting the TLR4 and NF-κB (Figure 4).

P2X7 mediated NLRP3 inflammasome activation is well documented in several studies.[17] A growing body of evidence suggested the involvement of NLRP3 and P2X7 in NAFLD and NASH.[43] P2X7 has also been associated with NOX activation. NOX-induced ROS formation and subsequent alteration in Kupffer cells have been shown to follow P2X7 stimulation by extracellular ATP. Additionally, ROS has been regarded as the shared property of inflammasome activation. ROS may serve as a "Kindling" factor to trigger NLRP3 inflammasome as well as act as an effector molecule for several signaling mediators. Results demonstrated that MLT could reduce NLRP3 activation through the modulation of the P2X7/NOX/ROS axis, suggesting a plausible mechanism for MLT-mediated inhibition of Steatohepatitis progression to fibrosis. The effect of MLT on P2X7 expression is yet to be reported in any diseased model. We, for the first time, reported that MLT could modulate P2X7 expression in high-fat diet-induced murine NASH (Figure 5). A decrease in iROS level followed by MLT treatment was attributed to decreased NOX production (Figure 6).

Fibrosis results from excess accumulation of extracellular matrix (ECM) following the activation and proliferation of hepatic stellate cells (HSCs).[61] Approximately all MMPs are known to play vital roles in liver fibrosis. MMP-2 subdues collagen type I expression and its deficiency seem to support intensified liver fibrosis. Although MMP-2, MMP-9 was most usually reported, MMPs related to the regulation of liver fibrogenesis seem to be linked to tissue remodeling during the progression of liver fibrosis.[62,63] Melatonin targets numerous molecular pathways, that reduce excessive fibrosis.[64] In our study, it is also noticed that MLT treatment reduced MMP2 and MMP9 levels with the subsequent increase of TIMP 1 indicating a reduction in collagen damage (Figure 8).

This is further justified by the Docking study where MLT shows a strong binding affinity for P2X7 (Figure 7). In vitro study reflected MLT suppresses Ca^{2+} level in parallel to P2X7 expression (Figure 5E and H). BBG, an inhibitor of P2X7 inhibited NLRP3 activation. This suggested that MLT inhibited NLRP3 through the suppression of P2X7. Inhibition of NLRP3 activation via P2X7 signaling by the natural compound curcumin in PMA-induced macrophages[65] corroborates our findings.

Conclusion

Melatonin ameliorates inflammation and other pathophysiological symptoms of NASH in a high-fat diet mice model by inhibiting NLRP3 inflammasome and its associated proteins via suppression of TLR4/NF-κB pathway and modulation of P2X7/NOX/ROS axis.

Acknowledgments

The authors gratefully acknowledge Smt. Banasri Das, Mr. Sounak Bhattacharya, Mr. Tanmoy Dalui, and Ms. Debalina Chakrabarty of the Central Instrumentation Facility, CSIR-Indian Institute of Chemical Biology, for providing confocal microscopy facilities and flow cytometry.

Ethics Approval

All animal experiments and protocols were allowed by the CSIR-IICB institutional animal ethics committee (IICB-AEC; registration no.: 147/1999/CPCSEA) registered under Social Justice and Empowerment Committee for Control and Supervision of Experiments on Animals (CPCSEA), and approved by the Committee for Control and Supervision of Experiments on Animals (Ministry of Environment, Forests and Climate Change, The Government of India). The authors state that they have obtained appropriate institutional review board approval or have followed the principles outlined in the Declaration of Helsinki for all animal experimental investigations.

Funding

The research is supported by CSIR, the Government of India. A research fellowship from DST–INSPIRE FELLOWSHIP scheme, Government of India to M. Saha is gratefully acknowledged. The authors are very grateful to the DST-SERB and DBT-NER Government of India for partial funding support.

Disclosure

The authors have read the journal's policy on disclosure of potential conflicts of interest and declare no conflicts of interest in relation to this work.

References

1. Grundy SM, Brewer HB, Cleeman JI, Smith SC, Lenfant C. Definition of metabolic syndrome: report of the national heart, lung, and serum institute/American Heart Association conference on scientific issues related to definition. *Circulation*. 2004;109(3):433–438. doi:10.1161/01.CIR.0000111245.75752.C6
2. Neuschwander-Tetri BA, Caldwell SH. Nonalcoholic steatohepatitis: summary of an AASLD single topic conference. *Hepatology*. 2003;37(5):1202–1219. doi:10.1053/jhep.2003.50193
3. Sayiner M, Koenig A, Henry L, Younossi ZM. Epidemiology of nonalcoholic fatty liver disease and nonalcoholic steatohepatitis in the United States and the rest of the world. *Clin Liver Dis*. 2016;20(2):205–214. doi:10.1016/j.cld.2015.10.001
4. Negro F. Natural history of NASH and HCC. *Liver Int*. 2020;40(S1):72–76. doi:10.1111/liv.14362
5. Lazo M, Hernaez R, Eberhardt MS, et al. Prevalence of nonalcoholic fatty liver disease in the United States: the third national health and nutrition examination survey, 1988–1994. *Am J Epidemiol*. 2013;178(1):38–45. doi:10.1093/aje/kws448

6. Fan JG. Impact of non-alcoholic fatty liver disease on accelerated metabolic complications. *J Dig Dis*. 2008;9(2):63–67. doi:10.1111/j.1751-2980.2008.00323.x
7. Boppidi H, Daram SR. Nonalcoholic fatty liver disease: hepatic manifestation of obesity and the metabolic syndrome. *Postgrad Med*. 2008;120 (2):1–3. doi:10.3810/pgm.2008.07.1800
8. Satapati S, Kucejova B, Shawn C, et al. Mitochondrial metabolism mediates oxidative stress and inflammation in fatty liver. *J Clin Invest*. 2016;125:4447–4462. doi:10.1172/JCI82204
9. Lebeaupin C, Vallée D, Hazari Y, Hetz C, Chevet E, Bailly-Maitre B. Endoplasmic reticulum stress signalling and the pathogenesis of non-alcoholic fatty liver disease. *J Hepatol*. 2018;69(4):927–947. doi:10.1016/j.jhep.2018.06.008
10. Chen Z, Tian R, She Z, Cai J, Li H. Corrigendum to "Role of oxidative stress in the pathogenesis of nonalcoholic fatty liver disease". *Free Radic Biol Med*. 2020;152:116–141. doi:10.1016/j.freeradbiomed.2020.06.011
11. Buzzetti E, Pinzani M, Tsochatzis EA. The multiple-hit pathogenesis of non-alcoholic fatty liver disease (NAFLD). *Metabolism*. 2016;65 (8):1038–1048. doi:10.1016/j.metabol.2015.12.012
12. Fang YL, Chen H, Wang CL, Liang L. Pathogenesis of non-alcoholic fatty liver disease in children and adolescence: from "two hit theory" to "multiple hit model". *World J Gastroenterol*. 2018;24(27):2974–2983. doi:10.3748/wjg.v24.i27.2974
13. Softic S, Cohen DE, Kahn CR. Role of dietary fructose and hepatic de novo lipogenesis in fatty liver disease. *Dig Dis Sci*. 2016;61(5):1282–1293. doi:10.1007/s10620-016-4054-0
14. Franchi L, Eigenbrod T, Muñoz-Planillo R, Nuñez G. The inflammasome: a caspase-1-activation platform that regulates immune responses and disease pathogenesis. *Nat Immunol*. 2009;10(3):241–247. doi:10.1038/ni.1703
15. Bawa M, Saraswat VA. Gut-liver axis: role of inflammasomes. *J Clin Exp Hepatol*. 2013;3(2):141–149. doi:10.1016/j.jceh.2013.03.225
16. Juliana C, Fernandes-Alnemri T, Kang S, Farias A, Qin F, Alnemri ES. Non-transcriptional priming and deubiquitination regulate NLRP3 inflammasome activation. *J Biol Chem*. 2012;287(43):36617–36622. doi:10.1074/jbc.M112.407130
17. Weber K, Schilling JD. Lysosomes integrate metabolic-inflammatory cross-talk in primary macrophage inflammasome activation. *J Biol Chem*. 2014;289(13):9158–9171. doi:10.1074/jbc.M113.531202
18. Franceschini A, Capece M, Chiozzi P, et al. The P2X7 receptor directly interacts with the NLRP3 inflammasome scaffold protein. *FASEB J*. 2015;29(6):2450–2461. doi:10.1096/fj.14-268714
19. Csak T, Ganz M, Pespisa J, Kodys K, Dolganiuc A, Szabo G. Fatty acid and endotoxin activate inflammasomes in mouse hepatocytes that release danger signals to stimulate immune cells. *Hepatology*. 2011;54(1):133–144. doi:10.1002/hep.24341
20. Wree A, McGeough MD, Peña CA, et al. NLRP3 inflammasome activation is required for fibrosis development in NAFLD. *J Mol Med*. 2014;92 (10):1069–1082. doi:10.1007/s00109-014-1170-1
21. Mridha AR, Wree A, Robertson AAB, et al. NLRP3 inflammasome blockade reduces liver inflammation and fibrosis in experimental NASH in mice. *J Hepatol*. 2017;66(5):1037–1046. doi:10.1016/j.jhep.2017.01.022
22. Thomas H. NAFLD: a critical role for the NLRP3 inflammasome in NASH. *Nat Rev Gastroenterol Hepatol*. 2017;14(4):197. doi:10.1038/nrgastro.2017.21
23. Zhao D, Yu Y, Shen Y, et al. Melatonin synthesis and function: evolutionary history in animals and plants. *Front Endocrinol (Lausanne)*. 2019;10:1–16. doi:10.3389/fendo.2019.00249
24. Tan D-X, Hardeland R, Manchester LC, et al. The changing biological roles of melatonin during evolution: from an antioxidant to signals of darkness, sexual selection and fitness. *Biol Rev*. 2010;85(3):607–623. doi:10.1111/j.1469-185X.2009.00118.x
25. Lochner A, Marais E, Huisamen B. Melatonin and cardioprotection against ischaemia/reperfusion injury: what's new? A review. *J Pineal Res*. 2018;65(1):1–22. doi:10.1111/jpi.12490
26. Sun H, Wang X, Chen J, et al. Melatonin improves non-alcoholic fatty liver disease via MAPK-JNK/P38 signaling in high-fat-diet-induced obese mice. *Lipids Health Dis*. 2016;15(1):1–8. doi:10.1186/s12944-016-0370-9
27. Hatzis G, Ziakas P, Kavantzas N, et al. Melatonin attenuates high fat diet-induced fatty liver disease in rats. *World J Hepatol*. 2013;5(4):160–169. doi:10.4254/wjh.v5.i4.160
28. Tahan V, Atug O, Akin H, et al. Melatonin ameliorates methionine- and choline-deficient diet-induced nonalcoholic steatohepatitis in rats. *J Pineal Res*. 2009;46(4):401–407. doi:10.1111/j.1600-079X.2009.00676.x
29. Gómez-Lechón MJ, Donato MT, Martínez-Romero A, Jiménez N, Castell JV, O'Connor JE. A human hepatocellular in vitro model to investigate steatosis. *Chem Biol Interact*. 2007;165(2):106–116. doi:10.1016/j.cbi.2006.11.004
30. Bort A, Sánchez BG, Spínola E, Mateos-Gómez PA, Rodríguez-Henche N, Díaz-Laviada I. The red pepper's spicy ingredient capsaicin activates AMPK in HepG2 cells through CaMKKβ. *PLoS One*. 2019;14(1):1–15. doi:10.1371/journal.pone.0211420
31. Jiang LH, Mackenzie AB, North RA, Surprenant A. Brilliant blue G selectively blocks ATP-gated rat P2X7 receptors. *Mol Pharmacol*. 2000;58 (1):82–88. doi:10.1124/mol.58.1.82
32. Pandey NR, Renwick J, Rabaa S, et al. An induction in hepatic HDL secretion associated with reduced ATPase expression. *Am J Pathol*. 2009;175 (4):1777–1787. doi:10.2353/ajpath.2009.090082
33. Dobashi H, Seki S, Habu Y, et al. Activation of mouse liver natural killer cells and NK1.1+ T cells by bacterial superantigen-primed Kupffer cells. *Hepatology*. 1999;30(2):430–436. doi:10.1002/hep.510300209
34. Jackson M, Taylor H, Jones E, Forrester LM. Mouse Cell Culture. *Methods Mol Biol*. 2010;633(1):29–56. doi:10.1007/978-1-59745-019-5
35. Aly FZ, Kleiner DE. Update on fatty liver disease and steatohepatitis. *Adv Anat Pathol*. 2011;18(4):294–300. doi:10.1097/PAP.0b013e318220f59b
36. Lanthier N. Targeting Kupffer cells in non-alcoholic fatty liver disease/ non-alcoholic steatohepatitis: why and how? *World J Hepatol*. 2015;7 (19):2184–2188. doi:10.4254/wjh.v7.i19.2184
37. Wan X, Xu C, Yu C, Li Y. Role of NLRP3 inflammasome in the progression of NAFLD to NASH. *Can J Gastroenterol Hepatol*. 2016;2016:1–7. doi:10.1155/2016/6489012
38. Friedman SL, Neuschwander-Tetri BA, Rinella M, Sanyal AJ. Mechanisms of NAFLD Development and Therapeutic Strategies. *Nat Med*. 2018;24 (7):908-922. doi:10.1038/s41591-018-0104-9
39. Rogero MM, Calder PC. Obesity, inflammation, toll-like receptor 4 and fatty acids. *Nutrients*. 2018;10(4):1–19. doi:10.3390/nu10040432
40. Shi H, Yin H, Flier JS, et al. TLR4 links innate immunity and fatty acid – induced insulin resistance. *J Clin Invest*. 2006;116(11):3015–3025. doi:10.1172/JCI28898

41. Velázquez-Miranda E, Díaz-Muñoz M, Vázquez-Cuevas FG. Purinergic signaling in hepatic disease. *Purinergic Signalling*. 2019;15(4):477–489. doi:10.1007/s11302-019-09680-3
42. Rossato M, Di Vincenzo A, Pagano C, El Hadi H, Vettor R. The P2X7 receptor and NLRP3 axis in non-alcoholic fatty liver disease: a brief review. *Cells*. 2020;9(4):1–12. doi:10.3390/cells9041047
43. Chatterjee S, Das S. P2X7 receptor as a key player in oxidative stress-driven cell fate in nonalcoholic steatohepatitis. *Oxid Med Cell Longev*. 2015;2015:1–7. doi:10.1155/2015/172493
44. Masarone M, Rosato V, Dallio M, et al. Role of oxidative stress in pathophysiology of nonalcoholic fatty liver disease. *Oxid Med Cell Longev*. 2018;2018:9547613. doi:10.1155/2018/9547613
45. Besse-Patin A, Estall JL. An intimate relationship between ros and insulin signalling: implications for antioxidant treatment of fatty liver disease. *Int J Cell Biol*. 2014;2014:519153. doi:10.1155/2014/519153
46. Delli Bovi AP, Marciano F, Mandato C, et al. Oxidative stress in non-alcoholic fatty liver disease. An updated mini review. *Front Med*. 2021;8:595371. doi:10.3389/fmed.2021.595371
47. Wang D, Wang H, Gao H, et al. P2X7 receptor mediates NLRP3 inflammasome activation in depression and diabetes. *Cell Biosci*. 2020;10(1):1–9. doi:10.1186/s13578-020-00388-1
48. Marchesini G, Day CP, Dufour JF, et al. EASL-EASD-EASO clinical practice guidelines for the management of non-alcoholic fatty liver disease. *J Hepatol*. 2016;64(6):1388–1402. doi:10.1016/j.jhep.2015.11.004
49. Zhang JJ, Meng X, Li Y, et al. Effects of melatonin on liver injuries and diseases. *Int J Mol Sci*. 2017;18(4):1–27. doi:10.3390/ijms18040673
50. García JA, Volt H, Venegas C, et al. Disruption of the NF-κB/NLRP3 connection by melatonin requires retinoid-related orphan receptor-a and blocks the septic response in mice. *FASEB J*. 2015;29(9):3863–3875. doi:10.1096/fj.15-273656
51. Farias da de SMT, Paixao da RI, MM Cruz, et al. Melatonin supplementation attenuates the pro-inflammatory adipokines expression in visceral fat from obese mice induced by a high-fat diet. *Cells*. 2019;8(9). doi:10.3390/cells8091041
52. Karolczak K, Watala C. The mystery behind the pineal gland: melatonin affects the metabolism of cholesterol. *Oxid Med Cell Longev*. 2019;2019:4531865. doi:10.1155/2019/4531865
53. Yu GM, Kubota H, Okita M, Maeda T. The anti-inflammatory and antioxidant effects of melatonin on LPS-stimulated bovine mammary epithelial cells. *PLoS One*. 2017;12(5):1–17. doi:10.1371/journal.pone.0178525
54. Seok JK, Kang HC, Cho YY, Lee HS, Lee JY. Therapeutic regulation of the NLRP3 inflammasome in chronic inflammatory diseases. *Arch Pharm Res*. 2021;44(1):16–35. doi:10.1007/s12272-021-01307-9
55. Xia MZ, Liang YL, Wang H, et al. Melatonin modulates TLR4-mediated inflammatory genes through MyD88- and TRIF-dependent signaling pathways in lipopolysaccharide-stimulated RAW264.7 cells. *J Pineal Res*. 2012;53(4):325–334. doi:10.1111/j.1600-079X.2012.01002.x
56. Chuffa GGA, Fioruci-Fontanelli BA, Mendes LO, et al. Melatonin attenuates the TLR4-mediated inflammatory response through MyD88- and TRIF-dependent signaling pathways in an in vivo model of ovarian cancer. *BMC Cancer*. 2015;15(1):1–13. doi:10.1186/s12885-015-1032-4
57. Bonomini F, Dos Santos M, Veronese FV, Rezzani R. NLRP3 inflammasome modulation by melatonin supplementation in chronic pristane-induced lupus nephritis. *Int J Mol Sci*. 2019;20(14):14. doi:10.3390/ijms20143466
58. Liu Y, Li C, Yin H, Zhang X, Li Y. NLRP3 inflammasome: a potential alternative therapy target for atherosclerosis. *Evidence-Based Complement Altern Med*. 2020;2020. doi:10.1155/2020/1561342.
59. Osier N, McGreevy E, Pham L, et al. Melatonin as a Therapy for Traumatic Brain Injury: A Review of Published Evidence. *Int J Mol Sci*.2018;19(5):1539. doi:10.3390/ijms19051539
60. Friedman SL. Mechanisms of hepatic fibrogenesis. *Gastroenterology*. 2008;134(6):1655–1669. doi:10.1053/j.gastro.2008.03.003
61. Naim A, Pan Q, Baig MS. Matrix Metalloproteinases (MMPs) in liver diseases. *J Clin Exp Hepatol*. 2017;7(4):367–372. doi:10.1016/j.jceh.2017.09.004
62. Roeb E. Matrix metalloproteinases and liver fibrosis (translational aspects). *Matrix Biol*. 2018;68–69:463–473. doi:10.1016/j.matbio.2017.12.012
63. Hu W, Ma Z, Jiang S, et al. Melatonin: the dawning of a treatment for fibrosis? *J Pineal Res*. 2016;60(2):121–131. doi:10.1111/jpi.12302
64. Wu X, Dong L, Lin X, Li J. Relevance of the NLRP3 inflammasome in the pathogenesis of chronic liver disease. *Front Immunol*. 2017;8. doi:10.3389/fimmu.2017.01728.
65. Kong F, Ye B, Cao J, et al. Curcumin represses NLRP3 inflammasome activation via TLR4/MyD88/NF-κB and P2X7R signaling in PMA-induced macrophages. *Front Pharmacol*. 2016;7:1–10. doi:10.3389/fphar.2016.00369